Exhumed mantle forming transitional crust in the Newfoundland-Iberia rift and associated magnetic anomalies.

J-C Sibuet,, S Srivastava,, Gianreto Manatschal

Exhumed mantle-forming transitional crust in the Newfoundland-Iberia rift and associated magnetic anomalies

Jean-Claude Sibuet,[1] Shiri Srivastava,[2] and Gianreto Manatschal[3]

Received 1 June 2005; revised 24 January 2007; accepted 12 February 2007; published 29 June 2007.

[1] Transitional zones located between Iberia and North America formed during continental rifting and mostly consist of exhumed mantle. In this study we show that ages of exhumed mantle at Ocean Drilling Program (ODP) sites 1068 and 1070 in the Iberia Abyssal Plain and site 1277 in the Newfoundland Basin are similar to ages determined from magnetic lineations created by serpentinization during mantle exhumation. On the basis of paleomagnetic and geological data and a comparison with a fossil ocean-continent transition in the Alps, we envisage a first episode of mantle serpentinization during which a strong component of magnetization was acquired followed by a second episode occurring at the contact with cold seawater, and which only affects the upper tens of meters of the exhumed mantle. The inversion of magnetic data (Euler deconvolution) shows that magnetic sources are N-S trending horizontal cylindrical bodies located within the highly serpentinized upper crust. Therefore the serpentinization process is able to produce magnetic lineations formed in a similar way to those formed by seafloor spreading. Within transition zones, sequences of magnetic anomalies can provide information concerning the timing of the emplacement of crust, but not on its nature (oceanic versus exhumed mantle). This discovery enables us to date the exhumation of mantle rocks in transition zones and allows kinematic reconstructions of the final stages of continental rifting. During rifting the deep distal continental margins and the adjacent transitional zones in the Newfoundland-Iberia rift system were formed by ultraslow extension from early Berriasian to late Valanginian–early Hauterivian and by slow extension from early Hauterivian to the late Aptian–early Albian boundary. Therefore transitional zones share many similarities with slow and ultraslow spreading midoceanic ridges.

Citation: Sibuet, J.-C., S. Srivastava, and G. Manatschal (2007), Exhumed mantle-forming transitional crust in the Newfoundland-Iberia rift and associated magnetic anomalies, *J. Geophys. Res.*, *112*, B06105, doi:10.1029/2005JB003856.

1. Introduction

[2] The Iberia Abyssal Plain (IAP) margin off Iberia is probably one of the best-studied magma-poor rifted margins in the world. Numerous multichannel seismic (MCS) cruises, detailed refraction surveys and drilling (Deep Sea Drilling Project (DSDP) leg 47B, Ocean Drilling Program (ODP) legs 149 and 173) have been carried out there. Yet, serious disagreements exist about the nature and mode of emplacement of the transitional crust, which lies between true continental and true oceanic crusts [e.g., *Dean et al.*, 2000; *Srivastava et al.*, 2000; *Whitmarsh et al.*, 2001a]. This transitional crust is regarded either to be strongly thinned continental crust through which the mantle was exhumed [*Dean et al.*, 2000; *Whitmarsh et al.*, 2001a] or to be a mixture of basalt, gabbro and mantle material, formed by ultraslow seafloor spreading [*Srivastava et al.*, 2000]. The prime objective of this paper is to show that these symmetrical magnetic lineations identified within the transitional zone between Iberia (IB) and North America (NA) are caused primarily by the serpentinization of the exposed mantle rocks within the 2–3 km of upper crust and not only by the magnetization of volcanic rocks formed by seafloor spreading. We will then explore the consequences of such findings and demonstrate that magnetic lineations can be used to quantify ages of emplacement of the crust and extension rates within transition zones.

[3] In this paper we use the expression "transitional zone" in the traditional sense (domain located between the distal thinned continental crust and the first typical oceanic crust). The transitional crust may consist of exhumed mantle but also of some decompression melting products. We also use in a restrictive sense the expression "seafloor spreading" as the extensional process, which results in the formation of typical oceanic crust generating conventional seafloor spreading magnetic anomalies. The *Kent and Gradstein* [1986] timescale is used throughout the

[1] Département des Géosciences Marines, Ifremer Centre de Brest, Plouzané, France.
[2] Geological Survey of Canada, Bedford Institute of Oceanography, Dartmouth, Nova Scotia, Canada.
[3] CGS-EOST, Université Louis Pasteur, Strasbourg, France.

0148-0227/07/2005JB003856$09.00

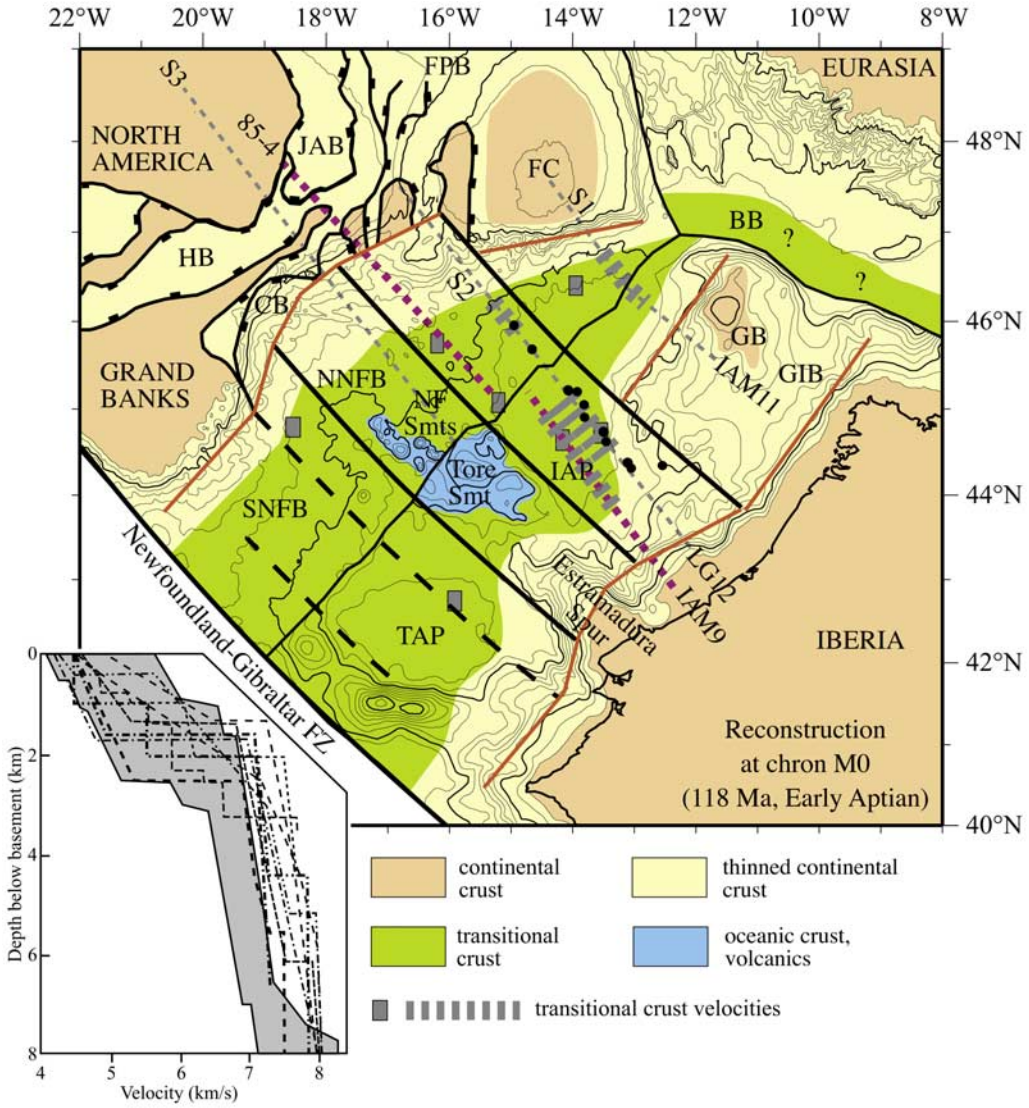

Figure 1. Plate reconstruction at chron M0 (118 Ma) with Eurasia (EU) kept fixed. Poles are from *Srivastava et al.* [2000] (Iberia (IB)/EU: 43.85°N, 5.83°W, −44.76°; North America (NA)/EU: 69.67°N, 154.26°E, 23.17°). Seismic lines IAM9 and Lithoprobe 85-4 are representative of the Iberian Abyssal Plain (IAP)/northern Newfoundland Basin (NNFB) conjugate margins. Location of published refraction results is shown with gray rectangles and thick gray hatchures). Black circles are Deep Sea Drilling Project (DSDP) and Ocean Drilling Program (ODP) sites in the IAP. Red lines are hinge lines determined from the crustal Bouguer gradients [*Sibuet et al.*, 2007]. Thick black lines are M25-M0 flow lines deduced from bathymetric, gravimetric, and magnetic data. BB: Bay of Biscay; CB: Carson Basin; FC: Flemish Cap; FPB: Flemish Pass Basin; GB: Galicia Bank; GIB: Galicia Interior Basin; HB: Horseshoe Basin; JAB: Jeanne d'Arc Basin; NF Smts: Newfoundland Seamounts; SNFB: southern Newfoundland Basin; TAP: Tagus Abyssal Plain. (inset, bottom left) Velocity versus depth below basement curves established from refraction and wide-angle seismic profiles located by gray rectangles [*Srivastava et al.*, 2000]. Given in gray are bounds for the 59–170 Ma Atlantic crust [*White et al.*, 1992].

paper to date the biostratigraphic stages and magnetic anomalies.

2. Kinematic Background

[4] To examine the symmetry of the transition zones across the North Atlantic we carried out a reconstruction of the North Atlantic with respect to Eurasia (EU) at the time of chron M0 (early Aptian, 118 Ma) [*Sibuet et al.*, 2004a, 2004b], M0 being regarded in the past as an undisputed oceanic magnetic anomaly formed by seafloor spreading (Figure 1). Hinge lines in orange were inferred from crustal Bouguer anomalies [*Sibuet et al.*, 2007] and correspond to the locations of the maximum slope of the Moho. Southwest of the Galicia Bank/SE Flemish Cap segment, the similar shapes of hinge lines on both sides of the transition zones and the constant distance between them (440 km) suggest that the domains formed in between

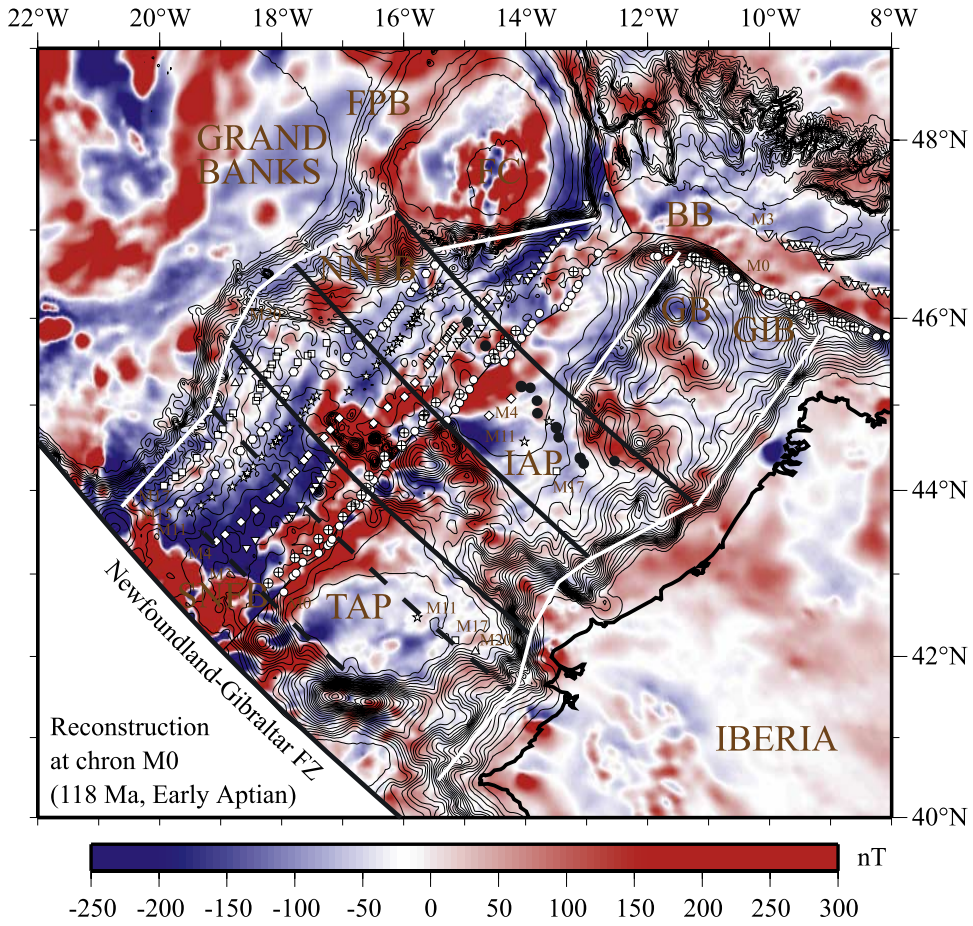

Figure 2. Magnetic anomalies [*Verhoef et al.*, 1996b] displayed on the plate reconstruction of west Iberia and NA conjugate margins at chron M0 (118 Ma) with EU kept fixed. Pole parameters and legend of symbols as in Figure 1. Magnetic picks from *Srivastava et al.* [2000] and *Sibuet et al.* [2004b]. White lines are hinge lines, and black lines are flow lines extracted from *Sibuet et al.* [2007].

were approximately symmetrical at the time of chron M0. Between hinge lines, the thick NW-SE black lines oriented parallel to the Newfoundland-Gibraltar fracture zone (FZ), correspond to chrons M25-M0 flow-lines and thus delineate the boundaries of the main conjugate segments between IB and NA margins [*Sibuet et al.*, 2007]. One can notice that the trend of chron M0 is approximately linear, contrasting with the broken trends of the hinge lines located immediately south of Flemish Cap and Galicia Bank. Thus a plate boundary reorganization probably occurred at the end of the main thinning episode of the continental margins, as attested by the trends of magnetic lineations within the transitional crust of the Iberia Abyssal Plain/northern Newfoundland Basin (IAP/NNFB) segment (Figure 2, for example), which are approximately parallel to chron M0. Consequently, from this kinematic framework at chron M0, it seems that the conjugate transitional domains are approximately symmetrical in this part of the North Atlantic.

3. Sea Surface and Deep-Tow Magnetic Data

[5] To test if symmetry exists in the magnetic data of the conjugate transition zones, we carried out a similar reconstruction of the North Atlantic at chron M0 using the compiled magnetic data of *Verhoef et al.* [1996a] (Figure 2). Except for some large amplitude anomalies, no sharp linear anomalies can be seen. This is because the anomalies generally have very small amplitudes and are obscured in this highly smoothed data set. On the other hand, the comparison of original profiled data (Figure 3) [*Srivastava et al.*, 2000] shows the presence of a number of seafloor spreading type anomalies, which appear in Figure 2 as a series of parallel magnetic lineations.

[6] Figure 3 displays three examples of conjugate magnetic anomaly profiles across IB/NA conjugate segments. Tracks on the NA side have been flipped over end-to-end to create their mirror images for easy comparison. Two of them concern the IAP/NNFB transect and include deep-tow magnetic data, and one of them concerns the Tagus Abyssal Plain/southern Newfoundland Basin transect. Several other similar conjugate magnetic profiles are displayed by *Srivastava et al.* [2000].

[7] Figure 3a displays the LG12 and ER56 conjugate profiles located within the IAP/NNFB segment. The towed ocean bottom instrument (TOBI) 91 deep-tow profile was acquired along profile LG12. The Sonar Acoustique Remorqué (SAR) 93 deep-tow profile, which is slightly oblique to the TOBI91 profile (location in Figure 4) is also shown as it was acquired along the western part of the IAP drilling transect. If we assume that magnetic anomalies are

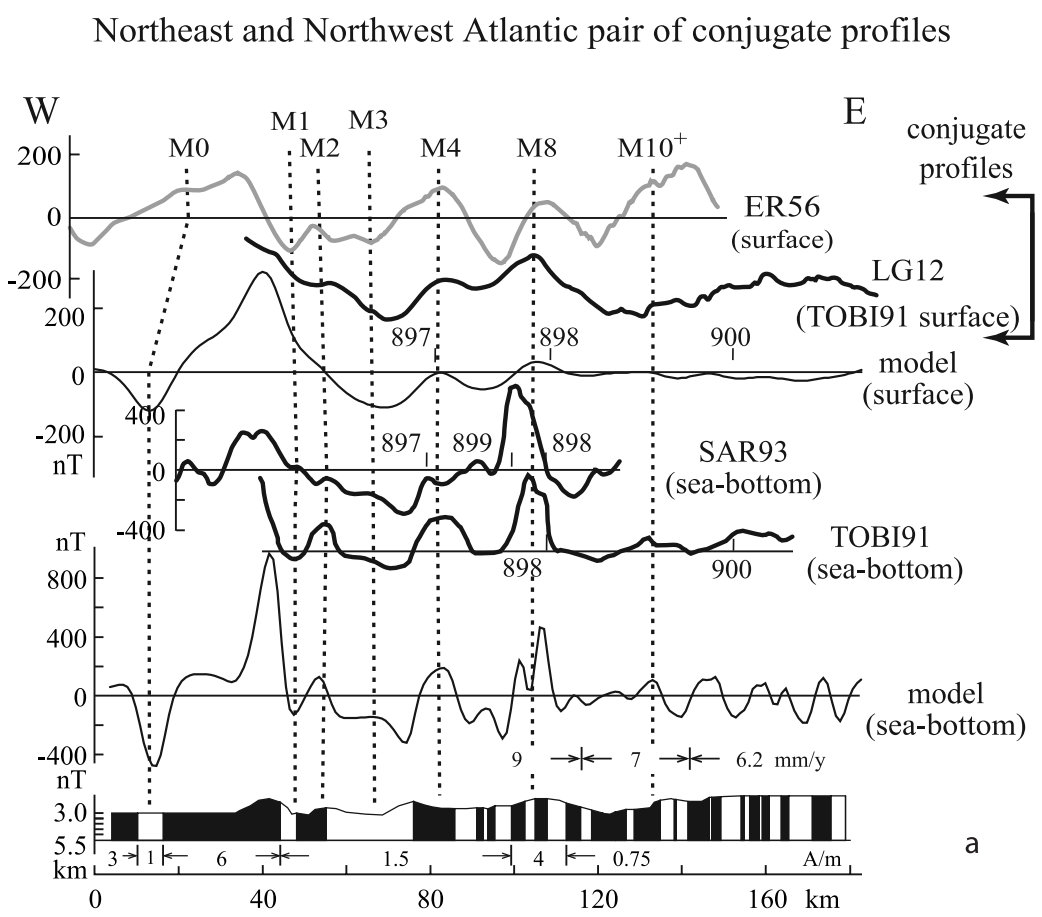

Figure 3. Correlation between observed and calculated M-sequence anomalies for conjugate magnetic profiles located in Figure 3b [*Srivastava et al.*, 2000]. Seafloor-spreading model with thickness of magnetic layer, magnetization, and velocities indicated at the bottom of Figures 3a and 3b. Other parameters as given by *Srivastava et al.* [2000]. Conjugate profiles on the NA side have been flipped end-to-end to create its mirror image for comparison. (a) ER56 and LG12 sea surface conjugate profiles [*Srivastava et al.*, 2000] with corresponding towed ocean bottom instrument (TOBI) 91 and Sonar Acoustique Remorqué (SAR) 93 deep-tow profiles [*Whitmarsh et al.*, 1996]. (b) ER33 and IAM9 conjugate profiles across the IAP and NNFB basins and 7(aero) and TAP 86-01 conjugate profiles across the Tagus and SNFB basins [*Srivastava et al.*, 2000]. Vertical scales are the same for all sea surface profiles.

seafloor spreading type anomalies, a very good correlation between deep-tow and calculated anomalies is obtained for anomalies ranging from M1 to M8. A comparison between sea surface data and calculated anomalies at the sea surface shows that anomalies M1 to M8 can also be easily recognized, but their identification is strengthened by the deep-tow anomalies forward modeling. This correlation rapidly deteriorates for older anomalies. The correlation with the conjugate ER56 profile is particularly good for anomalies M1 to M8 and becomes less clear for anomaly M10, though it may be correlated with the deep-tow M10 identification.

[8] Similarly, Figure 3b displays the IAM9/ER33 conjugate profiles within the IAP/NNFB segment and the TAP86-01 and 7(aero) conjugate profiles within the Tagus Abyssal Plain/southern Newfoundland Basin segment. The correlation between observed and calculated anomalies is good, even though spreading rates are slightly asymmetrical.

[9] In order to fit the amplitude of magnetic anomalies to model calculations, we had to vary the magnetization values locally from 0.75 to 8 A/m in the magnetized layer of constant thickness. It is unusual for a typical oceanic crust formed by seafloor spreading to have such varied magnetization values and this argument was extensively used by those arguing against seafloor spreading type anomalies in this region [e.g., *Russell and Whitmarsh*, 2003; *Whitmarsh et al.*, 2001b].

[10] From the above comparison between IB and NA magnetic data, M0 to M3 anomalies are of similar amplitude on both sides of the ocean [*Srivastava et al.*, 2000] but of half the amplitude of those in the central Atlantic Ocean [*Srivastava et al.*, 2000]. Magnetic lineations older than M3 between IB and NA [*Miles et al.*, 1996] are low in amplitude compared to their central Atlantic counterparts. In addition, they are higher in amplitude on the NA side than on the IB side where they are barely visible in sea surface data (Figure 3a). Though these anomalies are weak, they are symmetrical and bear all the characteristics of seafloor spreading anomalies, which led *Srivastava et al.* [2000] to identify them as part of the M-sequence anomalies. However, most scientists working in this area consider

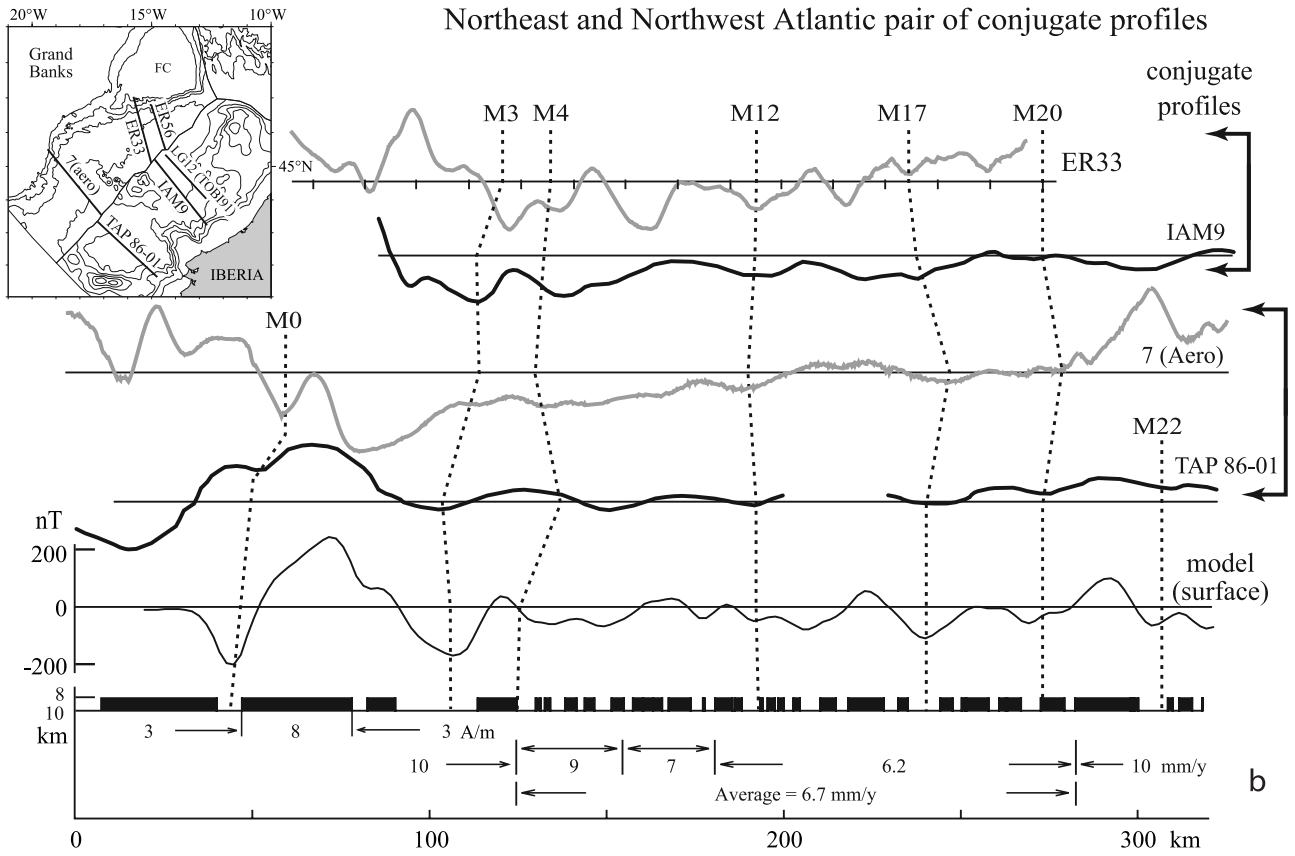

Figure 3. (continued)

that only magnetic anomalies younger than M3 or M5 are seafloor-spreading-type anomalies, even though they lie in regions underlain by a mixture of serpentinized peridotite and gabbros. Older magnetic lineations were either ignored or interpreted as synextensional deep elongated intrusions [e.g., *Russell and Whitmarsh*, 2003]. *Russell and Whitmarsh* [2003] argumentation is based on IAP refraction data [*Chian et al.*, 1999; *Dean et al.*, 2000], which displays velocities interpreted as serpentinized mantle east of the M3 lineation and oceanic crust to the west though the crustal thickness is reduced compared with the standard oceanic crust defined by *White et al.* [1992].

4. Depth of Magnetic Sources in the Iberia Abyssal Plain

[11] On the basis of the assumption of a uniformly magnetized basement, *Russell and Whitmarsh* [2003] and *Tucholke and Sibuet* [2007] show that the contribution of the basement topography is only ~10% of the amplitude of observed magnetic anomalies. Thus the observed IAP anomalies are largely due to magnetic contrasts within the crust itself. *Russell and Whitmarsh* [2003] estimated depths of magnetic sources by applying two techniques: the inversion of power spectra and a 3-D Euler deconvolution. Source depths were estimated from power spectra by fitting straight lines to band-limited segments for the three TOBI91, SAR93 and SAR95 deep-tow profiles. Sources 29 km below the deep-tows were found on the three profiles and are attributed to a component of the regional field that was not removed entirely in the attempt to separate the regional and residual fields [*Russell and Whitmarsh*, 2003]. Sources 4 km below the magnetometer of SAR95 profile (Figure 5b) are located in the upper crust. We suggest that the variations of power spectrum values around the 4-km straight line (Figure 5c) are due to lateral changes in upper crustal magnetization values. *Russell and Whitmarsh* [2003] also showed an additional source located 10.5 km below the magnetometer (6.5 km below the top of the basement, i.e., in the lower crust, Figure 5b). Figure 5c is identical to Figure 5b without the 10.5-km straight line suggesting that magnetic sources at that depth do not exist.

[12] Inversion of deep-tow magnetic profiles using the *Parker and Huestis* [1974] method for a 4-km thick layer and wavelengths of 25 km yields high magnetizations of 3–3.5 A/m in transition zones TZA and TZB and <1 A/m in TZC [*Russell and Whitmarsh*, 2003]. These values roughly correspond to the range of magnetizations independently used in the forward modeling of Figure 3.

[13] Euler solutions were computed for three structural indexes (0, 0.5, and 1) corresponding to semi-infinite, step and dyke-like contacts, respectively [*Russell and Whitmarsh*, 2003] (Figure 5d). Choosing the structural indexes may cause spatial diffusion of the Euler solutions and a bias in the depth estimates of magnetic sources. In addition, the problem becomes even more complicated when magnetic anomalies from two or more sources interfere. For the TOBI91 profile, we do not see any differences in character between TZA and TZB on one side and TZC and the thinned continental crust on the other side. The main

difference occurs at the boundary between TZB and TZC, which corresponds to the boundary between high- and low-amplitude magnetic anomalies and to the major change in basement depth (Figure 5a). From *Russell and Whitmarsh* [2003] results, it is impossible to document any change in nature and depth of magnetic sources within TZA and TZB as well as within TZC and the thinned adjacent continental crust. The interpretation of Figure 5e in terms of oceanic crust in TZA and gabbroic intrusions in TZB and TZC (Figure 5e) is not supported by Euler solutions. In addition, the SAR95 deep-tow profile does not seem to correspond to the IAM9 surface magnetic profile in term of upward prolongation (Figure 5e). This may be due to some problem in reducing the data for the SAR95 profile or a problem of correspondence between the location of deep-tow and surface profiles.

[14] The analytic signal and Euler deconvolution techniques are widely used to identify the locations and depths of sources independently of magnetization directions. We have used a combined inversion for the structural index and the source location from the Euler deconvolution, which only uses derivatives of magnetic anomalies [*Hsu*, 2002]. This approach considerably reduces the diffusion problem in location and depth solutions. Figure 6 shows the TOBI91 deep-tow profile of Figure 5d located in Figure 5a, with a 4 km upward prolongation to ensure a stable calculation. On the basis of the maximum amplitudes of the analytic signal [*Hsu et al.*, 1998], we can identify the spatial distribution of the main causative magnetic sources underlined by vertical dashed lines in Figure 6. If we use the new *Hsu* [2002] methodology, the location of magnetic sources agrees well with the maximum amplitude of the analytic signal. The three main sources are at depths of 0.5, 2 and 3 km beneath the acoustic basement and structural indexes are about 2. Knowing the structural index associated with each source, the interpretation of the Euler depths becomes easy and significant. The structural index of 2 [*Hsu*, 2002] corresponds to cylinders, which are probably horizontal and parallel to the IAP magnetic lineations, that is perpendicular to the direction of the profile. The depths of cylinder axes are at 0.5, 2 and 3 km beneath the top of the acoustic basement but we have no constrain on the diameters of cylinders.

[15] In conclusion, it seems unlikely that the observed magnetic anomalies are produced by elongated source bodies located within the lower crust, at about 6–8 km beneath the top of the basement but more likely by N-S trending horizontal cylindrical sources located at shallower depth within the 3 km of upper crust.

5. Serpentinization of Peridotites and Associated Magnetic Properties

[16] While unaltered peridotites have a weak magnetic susceptibility, extensively serpentinized peridotites have high magnetic susceptibilities and their magnetic behavior is ferromagnetic. This change in magnetic properties is due to the formation of magnetite during serpentinization [*Dunlop and Prévot*, 1982]. Magnetite is formed to host the excess iron that is released by ferromagnesian minerals (olivine and pyroxenes). In the course of serpentinization, peridotites also acquire a crystallization magnetic remanence because of the growth of newly formed magnetite grains in the ambient geomagnetic field [*Dunlop and Prévot*, 1982]. It has been proposed that the magnetic susceptibility of serpentinized peridotites increases linearly with the degree of serpentinization [*Bina and Henry*, 1990; *Nazarova*, 1994]. Recent studies show that this relationship is not linear [*Horen and Dubuisson*, 1995; *Keslo et al.*, 1996; *Toft et al.*, 1990]. An extensive study of abyssal peridotites [*Oufi et al.*, 2002] demonstrates that the magnetic susceptibility remains modest for low degrees of serpentinization (<75%) but increases rapidly for degrees of serpentinization higher than 75%. The formation of magnetite is related to the initial iron content of olivine and pyroxene minerals but the remanent magnetic properties of serpentinized peridotites are highly variable. High NRM values are linked to pseudo-single-domain range where elongated magnetite grains occur in the form of thin and closely spaced vein-like concentrations. Low NRM values are linked to multidomain range where magnetite grains occur in the form of irregular aggregate concentrations, which could promote magnetostatic interactions between grains [*Oufi et al.*, 2002].

[17] Thus the contribution of peridotites to magnetic anomalies becomes significant when they are affected by a high degree of serpentinization (>75%) [*Oufi et al.*, 2002] with irregular NRM values, which may exceed 5 A/m. Such highly serpentinized peridotites are characterized by seismic velocities of 5–5.5 km/s [*Christensen*, 1978; *Horen et al.*, 1996; *Miller and Christensen*, 1997]. Therefore the remanent magnetization carried by these highly serpentinized peridotites can be comparable to that of oceanic basalts. In the IAP, 5–5.5 km/s velocities have been observed in the upper 2 km of the transition zone (inset in Figure 1) and have been interpreted as highly (>75%) serpentinized mantle [*Chian et al.*, 1999; *Dean et al.*, 2000]. The rest of the crust is less serpentinized (<75%) and may contribute little to recorded marine magnetic anomalies. As for the seafloor spreading process, the crustal magnetization is mostly provided by the upper 2 km of crust, though some deeper contribution from less serpentinized mantle might be similar to the contribution of gabbroic oceanic crust. However, magnetic properties of extensively serpentinized peridotites can vary significantly depending on whether the peridotites have been maghemitized (on the seafloor or in a fault zone that provided a downgoing pathway for seawater), or whether the conditions of serpentinization allowed for the crystallization of iron-bearing silicates together with serpentine and magnetite, and on whether these conditions of

Figure 4. (top) Detailed magnetic anomaly map in the Iberia Abyssal Plain [*Miles et al.*, 1996] with locations of the TOBI and SAR deep-tow profiles (ABC and DB) equipped with fluxgate magnetometers [*Whitmarsh et al.*, 1996]. White circles: DSDP, and ODP sites drilled during legs 47B, 149, and 173. Magnetic lineations are identified according to *Srivastava et al.* [2000]. (bottom) Basement emplacement and seafloor spreading magnetic ages (see text for explanations). ABC and DB deep-tow and sea surface recorded magnetic profiles with the magnetic model of *Srivastava et al.* [2000]. Drilling sites appear on the basement depth profiles.

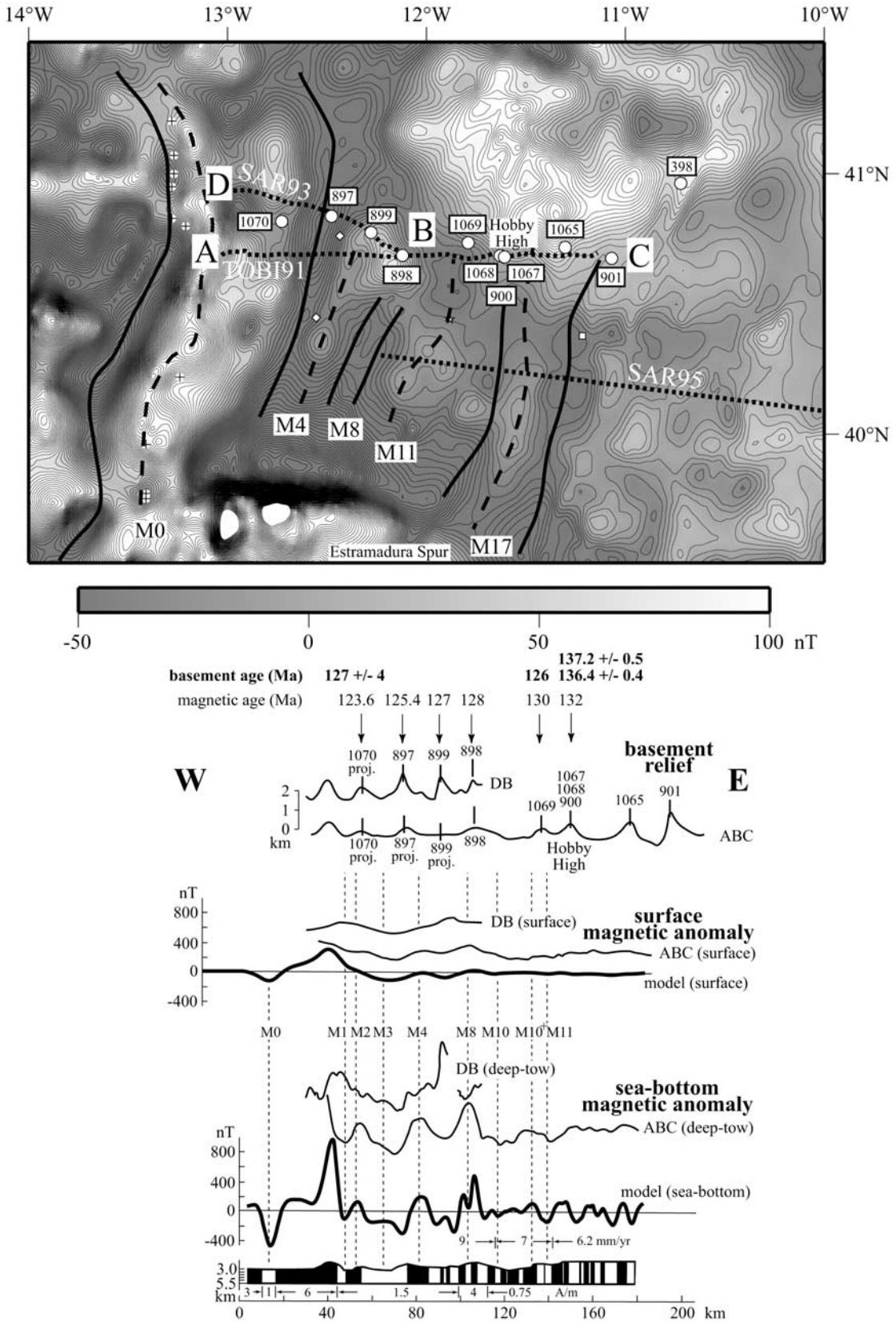
14°W
13°W
12°W
11°W
10°W
41°N
40°N
D
SAR93
A
TAB91
B
C
SAR95
897
899
1070
898
1069
Hobby
High
1065
1068
1067
900
901
398
M4
M8
M11
M0
M17
Estramadura Spur
-50
0
50
100 nT
basement age (Ma)
127 +/- 4
126
137.2 +/- 0.5
136.4 +/- 0.4
magnetic age (Ma)
123.6 125.4 127 128
130 132
W
E
basement relief
DB
ABC
km
Hobby High
nT
DB (surface)
surface magnetic anomaly
ABC (surface)
model (surface)
M0 M1 M2 M3 M4 M8 M10 M10 M11
DB (deep-tow)
sea-bottom magnetic anomaly
ABC (deep-tow)
model (sea-bottom)
6.2 mm/yr
A/m
0 40 80 120 160 200 km

Figure 4

serpentinization favored the formation of a serpentine meshwork with thin, vein-like concentrations or small and/or highly elongated magnetite grains [*Oufi et al.*, 2002]. Consequently, there is no reason to expect to have similar amplitude for magnetic anomalies over basaltic crusts formed by seafloor spreading and over serpentinized crust. In the IAP and NNFB transition zones, the amplitude of magnetic anomalies is small and the variable crustal magnetization values used in the magnetic model of Figure 3 attests of the high variability of the magnetization process.

6. Two Stages of Mantle Serpentinization

[18] *Manatschal* [2004] suggested that during the Valanginian, at the end of a main rifting phase in the IAP, a major tectonic event occurred and changed the geometry of faults from upward concave faults soling out at the crust-mantle boundary, to downward concave faults, which allowed exhumation of rocks from deep crustal levels and mantle without producing a major fault-bounded topography. Breccias and gouges in ODP holes show that the top of the basement represents a series of mantle detachments accommodating 10–20 km offsets [*Manatschal et al.*, 2001; *Whitmarsh et al.*, 2001a].

[19] Well-exposed examples of such structures are present in the Err/Platta nappes in the Alps (SE Switzerland) [*Froitzheim and Eberli*, 1990; *Manatschal and Nivergelt*, 1997]. In this area, low-angle detachment faults can be mapped and traced across a zone of exhumed mantle toward oceanic crust. On the basis of structural, mineralogical and geochemical investigations on the Err detachment fault, *Manatschal et al.* [2000] demonstrated that in the fault zones, the fluids triggered cataclastic deformation and mineral reactions allowing the identification of a mantle source for the fluids, which produced an enrichment of mantle-derived elements such as Cr and Ni. *Frueh-Green et al.* [2002] demonstrated that the serpentinization of mantle rocks resulted in high concentrations of Ni and Cr. Thus the enrichment in these elements along the Err detachment suggests that this fault cut into the mantle and that part of the serpentinization may have occurred before the mantle was exposed at the seafloor [*Manatschal*, 2004].

[20] We consequently propose a model in which the mantle exhumation occurs along downward concave faults, where mantle fluids, as well as seawater carried down from the seafloor, interact with mantle rocks, allowing mantle serpentinization to occur. In addition, because of the plate bending, open fractures were probably created as observed for example on oceanic crust bulges before their subduction [e.g., *Sibuet and Le Pichon*, 1971]. These may carry fluids deeply into the future exhumed mantle, allowing the chemical penetrative serpentinization, which occurs at temperatures below the Curie point, to propagate 2–3 km inside the mantle (Figure 7). The orientation of magnetite grains within the magnetic field follows the ambient magnetic field at crustal levels, during mantle cooling (Figure 7). Because of the high spatial variability of serpentinization, the crustal magnetization might be heterogeneous both vertically and horizontally, as suggested by forward magnetic modeling where the mean magnetization varies from 0.75 to 8 A/m. As soon as the serpentinized mantle becomes close to the seafloor or outcrops at the seafloor, the upper several tens of meters of serpentinized peridotite started to be altered by seawater (Fischer-Tropsch reaction), increasing the degree of serpentinization, with magnetite reacting to maghemite, a mineral whose magnetization is weak and which does not contribute significantly to the magnetic field.

7. Magnetization of Serpentinized Peridotites

[21] Direct evidence that serpentinite can contribute significantly to the magnetic field has been presented by *Zhao et al.* [1996, 2001, 2007a, 2007b] who studied heating and cooling curves of serpentinized peridotite samples from both the Iberia and Newfoundland transitional zones (ODP legs 149, 173 and 210). In general they show that the yellow and brown peridotite samples display Curie temperatures useful to determine the magnetic mineralogy around 420°C, indicative of the presence of maghemite responsible for the low natural remanent magnetization ($\sim$1 A/m) and that gray and green peridotite samples display Curie temperatures around 570°C indicative of the presence of magnetite and high remanent magnetization (up to 9 A/m). These values of remanent magnetization

Figure 5. (a) Depth to basement chart on a 500-m grid [*Russell and Whitmarsh*, 2003] and bathymetric contours from *Sibuet et al.* [2004a] showing portions of the transition zone (TZA, TZB, and TZC) bounded by dotted lines. Bold lines denote three SAR and TOBI deep-tow tracks; thin lines correspond to wide-angle seismic lines [*Chian et al.*, 1999; *Dean et al.*, 2000]. Red triangles are peridotite ridges R3 and R4. (b) Logarithms of the power spectrum calculated from the total field anomaly along deep-tow magnetometer profile SAR95 [*Russell and Whitmarsh*, 2003] using *Spector and Grant*'s [1970] method. Using an average fish height of 4 km above the basement, three sources were modeled and found to be at 4 km (top of the basement), 10.5 km (6.5 km below the top of basement), and 29 km (25 km below the top of the basement) [*Russell and Whitmarsh*, 2003]. The deepest source is an artifact attributed to the regional field component of the total field anomaly. (c) Same as Figure 5b, except that the straight line at 10.5 km has been removed. Undulations in the data are probably due to upper crustal variations in magnetization values. (d) Euler deconvolution of magnetic anomalies along deep-tow profile TOBI91 for structural indexes of 0 (semi-infinite contact: red circles), 0.5 (step contact: green diamonds), and 1.0 (dyke-like contact: blue squares) [*Russell and Whitmarsh*, 2003]. The main boundary is between TZB and TZC. (e) (top) Magnetic model along the deep-tow profile SAR95, coincident with the multichannel seismic (MCS) profile IAM9 from *Russell and Whitmarsh* [2003]. Note the discrepancy between the surface and deep-tow profiles. (bottom) Magnetic model showing the base of crustal magnetic layer (lower dashed line), seafloor spreading blocks (±0.8 A/m), continental crust (0.1 A/m, stippled), undefined magnetic bodies (−0.8 A/m, gray), and a nonmagnetic block R3 [*Russell and Whitmarsh*, 2003]. Magnetization values are from *Van der Voo* [1990] ($I_M = 46°$; $D_M = 0°$).

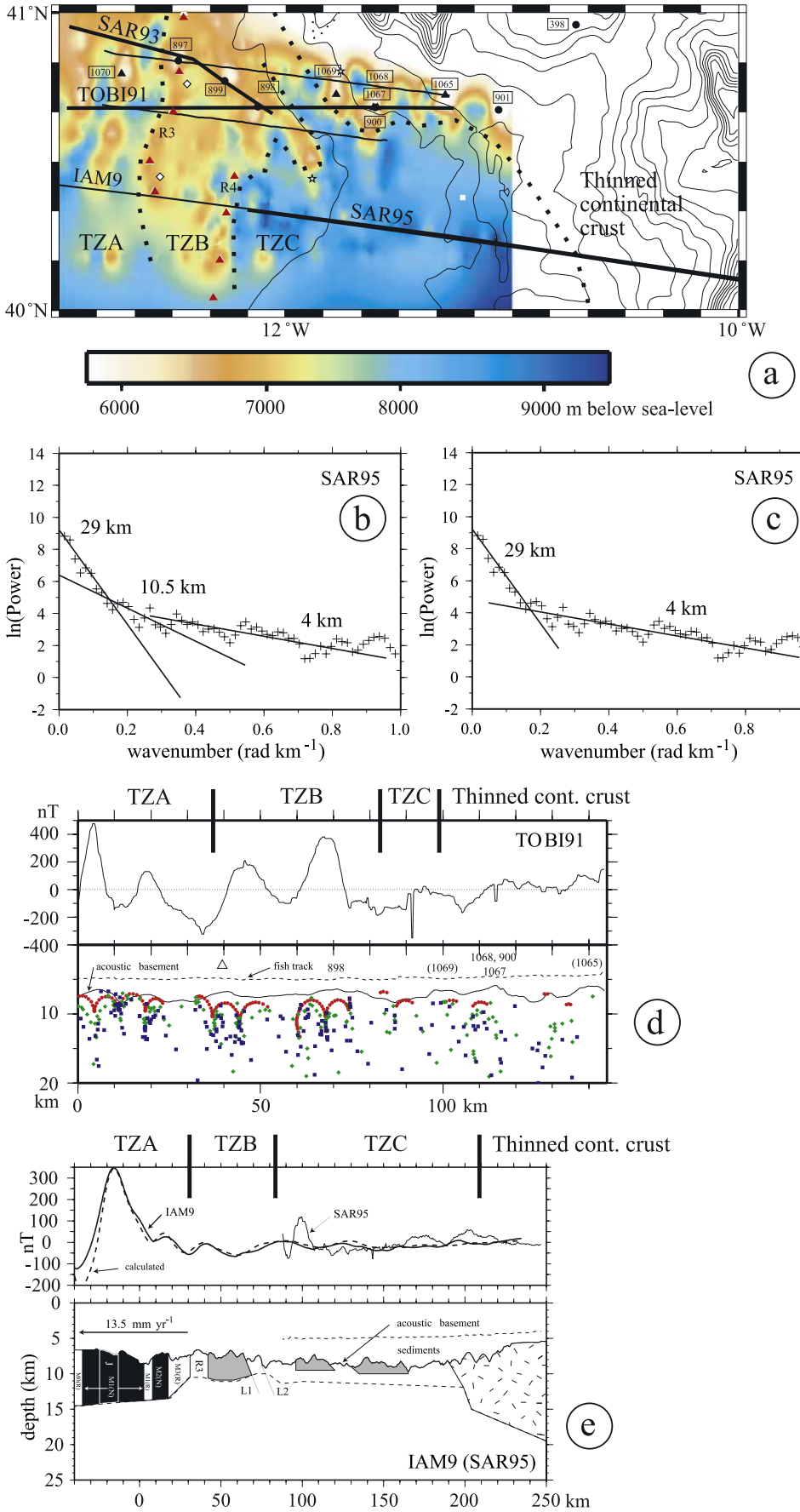
41°N
40°N
12°W
10°W
SAR93
TOBI91
IAM9
SAR95
R3
R4
TZA
TZB
TZC
Thinned continental crust
897
898
899
900
901
1065
1067
1068
1069
1070
398
6000
7000
8000
9000 m below sea-level
a
SAR95
b
29 km
10.5 km
4 km
ln(Power)
wavenumber (rad km-1)
SAR95
c
29 km
4 km
ln(Power)
wavenumber (rad km-1)
TZA
TZB
TZC
Thinned cont. crust
nT
TOBI91
acoustic basement
fish track
898
(1069)
1068, 900
1067
(1065)
d
km
0
50
100 km
TZA
TZB
TZC
Thinned cont. crust
IAM9
SAR95
calculated
nT
13.5 mm yr-1
acoustic basement
sediments
R3
L1
L2
depth (km)
e
IAM9 (SAR95)
0
50
100
150
200
250 km

Figure 5

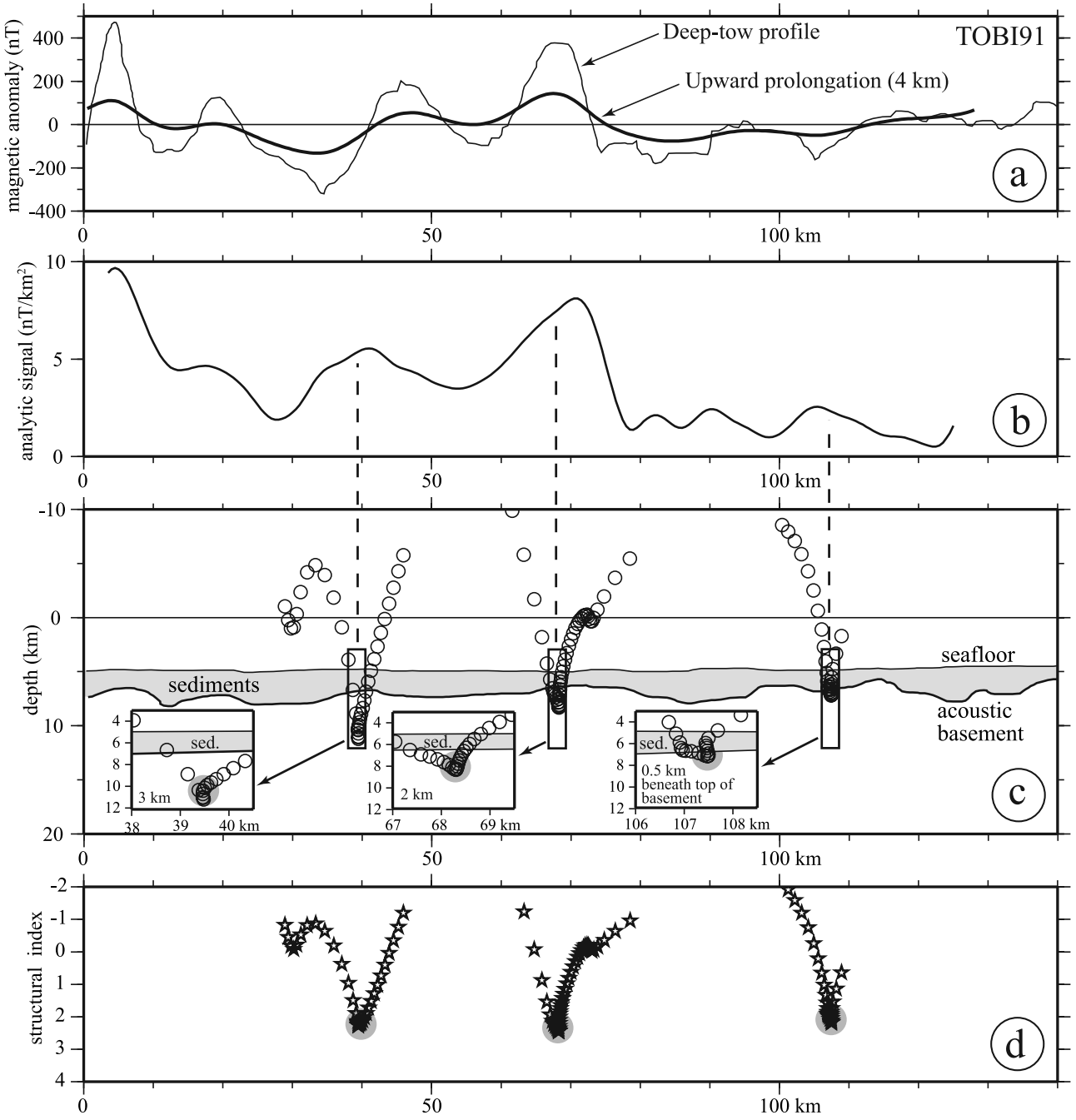

Figure 6. (a) TOBI91 deep-tow profile of Figure 5d with upward continuation (4 km) in order to remove the noise and inappropriate Euler solutions. (b) Analytic signal computed from the upward continued anomaly. (c) Calculated depth solutions using the *Hsu* [2002] method. The depth cluster solutions correspond to the light gray circles in the insets. (d) Structural indexes are calculated simultaneously. The solutions correspond to the light gray circles with structural indexes around 2 (cylinders whose axes are at the depth of the depth solutions [*Hsu*, 2002]).

are comparable to or higher than those of oceanic basalts. In addition, temperature hysteresis loop parameters, useful to estimate the domain structure of magnetic minerals, indicate that the peridotite sections on both sides of the Newfoundland-Iberia rift are compatible with the presence of pseudo single-domain grains. All samples show inclinations close to the theoretically predicted values for the paleolatitude of drilling sites, indicating that natural remanent magnetization (NRM) intensities probably represent the primary magnetization.

[22] On the Iberian side, relatively strong mean NRM intensities of 0.35, 1.8 and 1.6 A/m and mean values of the magnetic susceptibility of 2.1, 2.9 and 2.9 10^{-2} SI units [*Zhao*, 2001] are measured on samples from holes 897D, 899B, and 1070A, respectively, with variations in magnetic susceptibility which mimic those of the NRM intensity

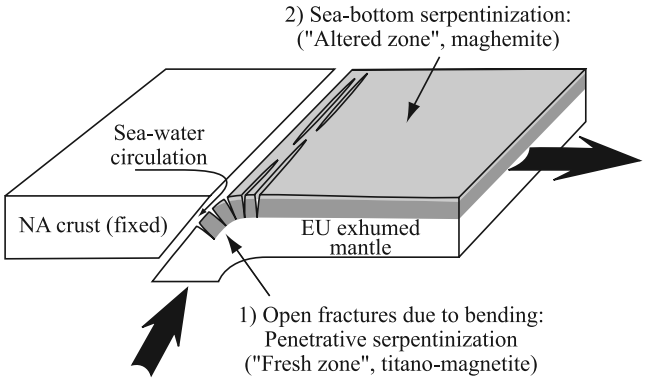

Figure 7. Two stages model of serpentinization processes: (1) Because of the bending of the exhumed mantle, open fissures on the outer part of the hinge allow seawater to deeply penetrate (2–3 km) and to serpentinize the mantle. During serpentinization, magnetite grains are oriented in the ambient magnetic field. (2) As soon as the serpentinized mantle outcrops at the sea bottom, the upper several tens of meters started to be altered by seawater (Fischer-Tropsch reaction).

(Figure 8). The stronger magnetization intensity at site 899 is in agreement with the presence of the large magnetic anomaly recorded on a deep-tow profile (Figure 4). In addition, several samples from hole 899B retained nearly half of their NRM intensity after 400°C demagnetization, suggesting that the remanence of the serpentinized ridge at this site can contribute significantly to the strong 800 nT magnetic anomaly recorded by the SAR deep-tow magnetometer [*Whitmarsh et al.*, 1996] (deep-tow profile DB in Figure 4). At all the three sites we observed the presence of a yellow-brown "altered" zone where maghemite is probably present, 40 to 75 m thick, with predominantly normal polarity overlying a gray-green "fresh" zone where magnetite is probably present [*Zhao*, 2001].

[23] On the Newfoundland side, paleomagnetic data at site 1277 indicate that the yellow-brown and gray-green serpentinized peridotites present Curie temperatures of 420°C and between 550 and 580°C indicative of the presence of maghemite and magnetite, respectively. High NRM intensities up to 9 A/m in the gray-green serpentinized peridotites probably explain the large amplitude of observed sea surface magnetic anomalies [*Zhao et al.*, 2007a].

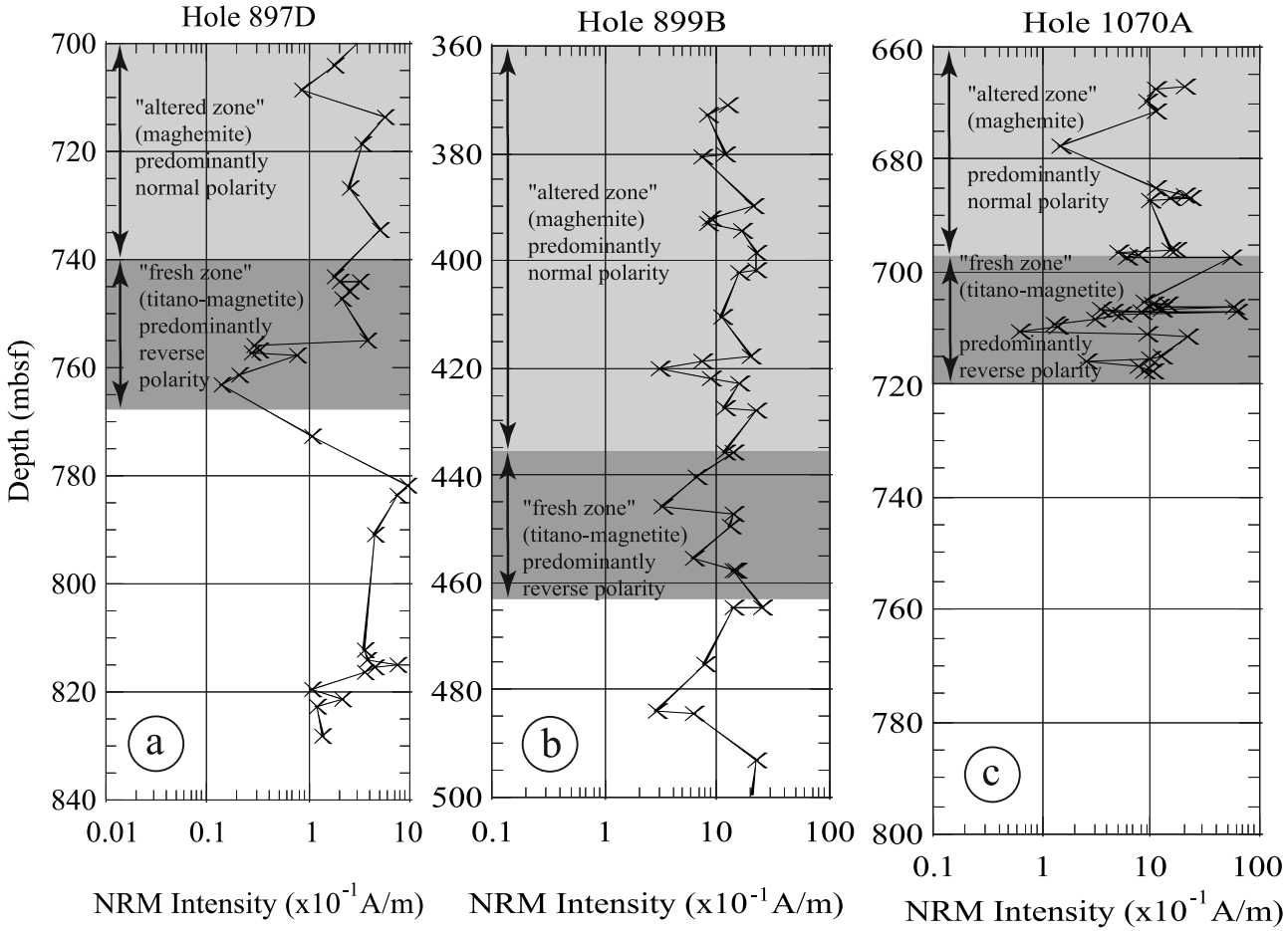

Figure 8. NRM intensities plotted against depth below serpentinized peridotite basement in ODP holes 897D, 899B, and 1070A (locations in Figure 4). Dark gray areas correspond to "fresh" gray-green serpentinites associated with a predominantly reverse magnetic polarity zone. Above, light gray areas correspond to "altered" yellow-brown serpentinites with predominantly normal polarity zone. Magnetic minerals are mostly maghemite in the "altered" zone and magnetite in the "fresh" zone [*Zhao*, 2001].

[24] Oxygen isotope profiles of serpentinized peridotites at sites 1068 and 1070 show evidence for two phases of serpentinization [*Skelton and Valley*, 2000] The first event (>175°C) involved a pervasive infiltration and a bulk serpentinization that is interpreted to occur before exhumation at the seafloor. The second event (<50°C) occurred at or close to the seafloor. Consequently, the strong magnetization at the three sites was first acquired in depth during an initial phase of serpentinization, at the time of emplacement and cooling of gray-green mantle peridotites, which recorded the polarity of the ambient magnetic field. The second phase of serpentinization occurred near or at the seafloor during final exhumation. It affected only the uppermost part of the peridotite bodies that was ''altered'' at the contact with the sea bottom water by a slow serpentinization process, giving rise to maghemitization. This is confirmed by paleomagnetic results, which show that the yellow-brown ''altered'' zone acquired its final magnetization later than the gray-green ''fresh'' zone [*Zhao*, 2001].

[25] On the basis of the above discussion, the serpentinization process may explain the magnetization responsible for magnetic anomalies in the transition zones. In this model, faults and open fractures caused by plate bending carried fluids deep into the exhuming mantle, allowing serpentinization to propagate to depths up to 2–3 km. Pseudo-single-domain magnetic grains in gray-green serpentinites became oriented along the magnetic field below the Curie temperature (570°C) by chemical reaction, recording the ambient magnetic field as the mantle cooled at crustal levels. There was probably a strong spatial variability in serpentinization, so crustal magnetization was vertically and horizontally heterogeneous, consistent with forward modeling where the mean magnetization varies from 0.75 to 8 A/m (Figure 3).

8. Comparison Between Ages of Mantle Exhumation Obtained From Drilling Results and Magnetic Anomalies

[26] Serpentinized peridotites were drilled in the IAP at ODP sites 897, 899, 1068, and 1070 and in the Newfoundland Basin at ODP site 1277. At site 1070, the top of the basement consists of calcite-cemented serpentinite breccias (comparable with ophicalcites in Alpine ophiolites [e.g., *Lemoine et al.*, 1987], which grade downward into serpentinized mantle intruded by a relatively fresh gabbro pegmatite dike [*Whitmarsh et al.*, 1998]. Clasts of pegmatoidal gabbro and albitite occur also in the upper breccia. U/Pb ages on zircon from the albitites at site 1070 gave 127 ± 4 Ma [*Beard et al.*, 2003], which is interpreted as the crystallization and emplacement age of the albitites.

[27] The metagabbros at site 900, less than 1 km from the drilled mantle at site 1068, were interpreted as underplated gabbros below a 24 km thick continental crust [*Cornen et al.*, 1999]. $^{40}Ar/^{39}Ar$ ages on plagioclase from these gabbros, gave 136.4 ± 0.3 Ma [*Féraud et al.*, 1996], which is a maximum age for the emplacement of these gabbros at site 900. Close to these sites, amphibolites were drilled at site 1067. U/Pb SHRIMP ages from one tonalite dike in the amphibolites gave Paleozoic ages, clearly indicating that the basement at this site is continental. $^{40}Ar/^{39}Ar$ ages on plagioclase from the amphibolites gave 137.2 ± 0.5 Ma [*Manatschal et al.*, 2001], i.e., ages identical to those obtained from the nearby gabbros at site 900. Therefore the $^{40}Ar/^{39}Ar$ ages on plagioclase from these two sites are interpreted as cooling ages below 150°C, predating the exhumation age of the rocks drilled at Hobby High, including the mantle rocks.

[28] At site 1069, a condensed sequence of Tithonian silty clays overlain by slumped upper Berriasian chalks with pebbles of limestones and metasediment and Valanginian chalks was drilled, documenting the stratigraphic record of continental breakup [*Wilson et al.*, 2001]. On the basis of benthic foraminiferal assemblages, *Urquhart* [2001] and *Kuhnt and Urquhart* [2001] suggested a paleowater depth of about 1500 m during Valanginian. The change in the supply of terrigenous sediments from Tithonian silty clays to Berriasian and Valanginian chalks was interpreted by *Wilson et al.* [2001] as linked to rift development that pond back turbidites upstream, suggesting that the first main rifting phase at site 1069 might have ended at 126 Ma, giving a minimum age for this site. The deepening in Valanginian is not an argument as strong as those obtained at site 1070 and Hobby High but data at site 1069 supports the overall trend.

[29] In the Newfoundland Basin, at site 1277, the serpentinized peridotite basement was intruded by an alkaline gabbro dike at 126.6 ± 4.0 Ma [*Jagoutz et al.*, 2007].

[30] These ages constrain the timing of mantle exhumation in the Newfoundland-Iberia transition zone, which is at present the only example worldwide where this process was dated. On land, in the ancient transition zone in the Alps, which can be considered an analog to the transition zone off Iberia [e.g., *Manatschal*, 2004], mantle exhumation has been dated by the oldest biostratigraphic ages obtained from the sediments sealing mantle rocks and adjacent oceanic and continental crusts. Ages for these overlying sediments range between Bathonian and Callovian (168–161 Ma) [*Bill et al.*, 2001]. U/Pb zircon ages on gabbros from the transition zone range between 165 and 157 Ma for the gabbros [*Lombardo et al.*, 2002; *Schaltegger et al.*, 2002] and $^{40}Ar/^{39}Ar$ cooling ages on phlogopite in a pyroxenite of the Totalp serpentinite yield a cooling age of 160 ± 8 Ma [*Peters and Stettler*, 1987]. Thus all these ages imply that exhumation and cooling of the mantle were associated with the exhumation of gabbros and albitite at the seafloor [*Manatschal*, 2004].

[31] The surface magnetic anomaly map of Figure 4 (top) is based on a much denser grid of data [*Miles et al.*, 1996] than the one used in Figure 2. It shows ~100-km-long N000° to N015° trending lineations in the IAP, between the southern part of Galicia Bank in the north and the Estramadura Spur in the south. Labels on magnetic lineations are those which correspond to magnetic anomalies identified by *Srivastava et al.* [2000] (Figure 4, bottom). Sites located east of site 898 are on the extreme northern side of the linear magnetic pattern. Sites 898 and 899 are located on an irregular positive magnetic anomaly located north of the N-S magnetic pattern. West of site 897 and west of Galicia Bank, magnetic lineations are extending northward. Figure 4 (bottom) shows ABC and DB lines across ODP sites along which deep-tow and surface magnetic measurements were carried out. Note that the deep-tow profile DB only partly

mimics the corresponding part of the ABC profile. The large positive anomaly associated with the ridge or seamount drilled at site 899, as well as the positive anomaly associated with the western seamount of the DB section, do not have any corresponding feature on the ABC profile. This means that the IAP drilling transect might be not fully representative of the overall IAP segment defined by the magnetic pattern of Figure 4.

[32] Ages of basement exhumation together with ages given by seafloor spreading magnetic anomalies appear in Figure 4. At site 1070, the 123.6 Ma age deduced from magnetic data modeling at this site is close to U/Pb age of 127 ± 4 Ma obtained for a gabbroic intrusion through the mantle peridotite at this site. At Hobby High (sites 1067, 1068, and 900), the 132 Ma age deduced from magnetic data is slightly younger than the $^{40}Ar/^{39}Ar$ cooling ages of 136.4 ± 0.3 Ma and 137.2 ± 0.5 Ma obtained from plagioclases in the gabbros (site 900) and the amphibolites (site 1067). However, if these rocks cooled at 136.4 Ma below 150°C, their exhumation at the seafloor is consequently younger. Assuming a normal thermal gradient of 30°C/km, an exhumation fault with an average dip of 30° and velocities of about 10 mm/yr, the emplacement of the gabbros and amphibolites occurred about 1 Ma after cooling at 150°C (~5 km depth), i.e., at about 135 Ma. In the Newfoundland Basin, at site 1277 located ~10 km east of M1 the corresponding age of 122 Ma on the *Kent and Gradstein* [1986] timescale has to be compared with the 126.6 ± 4.0 Ma age obtained on an alkaline gabbro dike.

[33] Consequently, ages obtained from magnetic modeling are systematically ~4 Ma younger than those obtained by geochronological measurements. Part of this discrepancy might be due to the time required for the exhumation of serpentinized peridotites (~1 Ma) as previously suggested but most of it is probably due to timescales conversion errors. Compared to the ages given by the *Kent and Gradstein* [1986] timescale, the *Gradstein et al.* [1995, 2004] and *Fiet et al.* [2006] timescales give magnetic ages 2 and 4 Ma older and 6 Ma younger, respectively. Taking into account errors on magnetic ages due to the used timescales (range of 10 Ma) and on geochronological ages, there is a good agreement between the ages of basement emplacement deduced from ages of magnetic anomalies and those measured on drilled samples. We suggest that during the process of mantle exhumation, magnetic lineations form in a similar way as basaltic oceanic crust is emplaced at a midocean ridges, with the difference however, that the resulting remanent magnetic field is much weaker.

9. Spreading/Extension Rates and Melt Supply

[34] Assuming that magnetic anomaly picks of *Srivastava et al.* [2000] are correct, half extension/spreading rates calculated by using the *Kent and Gradstein* [1986] timescale are 6–7 mm/yr for the period older than M8–M10 (late Valanginian-early Hauterivian, ~130 Ma), 9–10 mm/yr from M8–M10 to M3 (late Hauterivian, ~127 Ma) and 10–12 mm/yr from M3 to the Aptian/Albian boundary (113 Ma). The 10–12 mm/yr value is interpolated between chrons C34 and M0. If we used the *Gradstein et al.* [1995, 2004] and *Fiet et al.* [2006] timescales, half extension/spreading rates are slightly different [*Tucholke and Sibuet*, 2007]. Rates calculated for chrons older than M8–M10 are generally consistent at 6–7 mm/yr, except a large 13 mm/yr excursion at chron M11 for the *Gradstein et al.* [2004] timescale that probably is not real, reflecting a potential problem with this timescale. For the *Gradstein et al.* [1995, 2004] timescales, rates increased from 9 to 13 mm/yr between chrons M8–M10 and M3 and then remain approximately constant (13 mm/yr) from chrons M3 to C34 [*Tucholke and Sibuet*, 2007].

[35] Figure 9 shows the results from wide-angle reflection and refraction measurements carried out along conjugate profiles AGC 85-4 in the NNFB [*Keen and de Voogd*, 1988] and IAM9 in the IAP [*Pickup et al.*, 1996] located in Figures 1 and 10 (thick purple dashed lines). The line drawing of the corresponding MCS profiles has been superimposed. Crustal and sedimentary velocities were extracted from the data set of L. Matias (personal communication, 1999) for the thinned IB continental crust, *Dean et al.* [2000] for the IAP portion of the profile, and I. Reid (personal communication, 1992) for preliminary results of the *Erable* cruise concerning the eastern portion of the northern Newfoundland Basin. Data from *Reid and Keen* [1988] and *Reid* [1994] were used for the general velocity structure of the rest of the NNFB transitional crust and Grand Banks. The MCS data have been converted into depth profiles by using the above-mentioned velocities and the main layers have been defined from the geometry of reflectors and refraction velocity contrasts. We have added the location of magnetic identifications and half spreading/extension rates previously defined by using the *Kent and Gradstein* [1986] timescale. Surprisingly, a remarkable gross symmetry characterizes the magnetic structure of the cross section of Figure 9. On both sides of the ocean, the thinned continental domains are symmetrical and dips of continental slopes are similar (Figure 9), which is unusual as thinned conjugate continental crusts are generally asymmetrical [*Sibuet*, 1987]. The transitional zone consists of several subdomains named transitional zones TZA, TZB and TZC. TZCs consist of 100–120 km wide segments where near-symmetrical magnetic anomalies M8–M10 to M17 have been identified. Half extension/spreading rate is 6–7 mm/yr. The mean basement depth on the Iberia side is ~8.5 km. TZBs on each side of the ocean, about 40–50 km wide, consist of linear peridotite ridges on the IB side, and we postulate it is the same on the NA side. Basement depths are similar on both sides of the ocean (~7 km) (Figure 9). More or less symmetrical magnetic anomalies M3 to M8–M10 were recognized and the half extension/spreading rate is 9–10 mm/yr. The youngest TZA, where symmetrical magnetic anomalies younger than M3 were recognized, still present the petrological characteristics of a transitional domain as established by drilling at ODP sites 1070 and 1277. Half extension/spreading rate is 10–12 mm/yr and the mean basement depth is ~7 km, as for TZBs. In conclusion, combined reflection, refraction and magnetic data suggest the presence of roughly symmetrical conjugate transitional domains.

[36] Figure 10 shows the basement shape established from MCS data collected in the IAP [*Russell and Whitmarsh*, 2003] converted in depth by using refraction data [*Chian et al.*, 1999; *Dean et al.*, 2000], and in the northern Newfoundland Basin around MCS SCREECH line 2 with

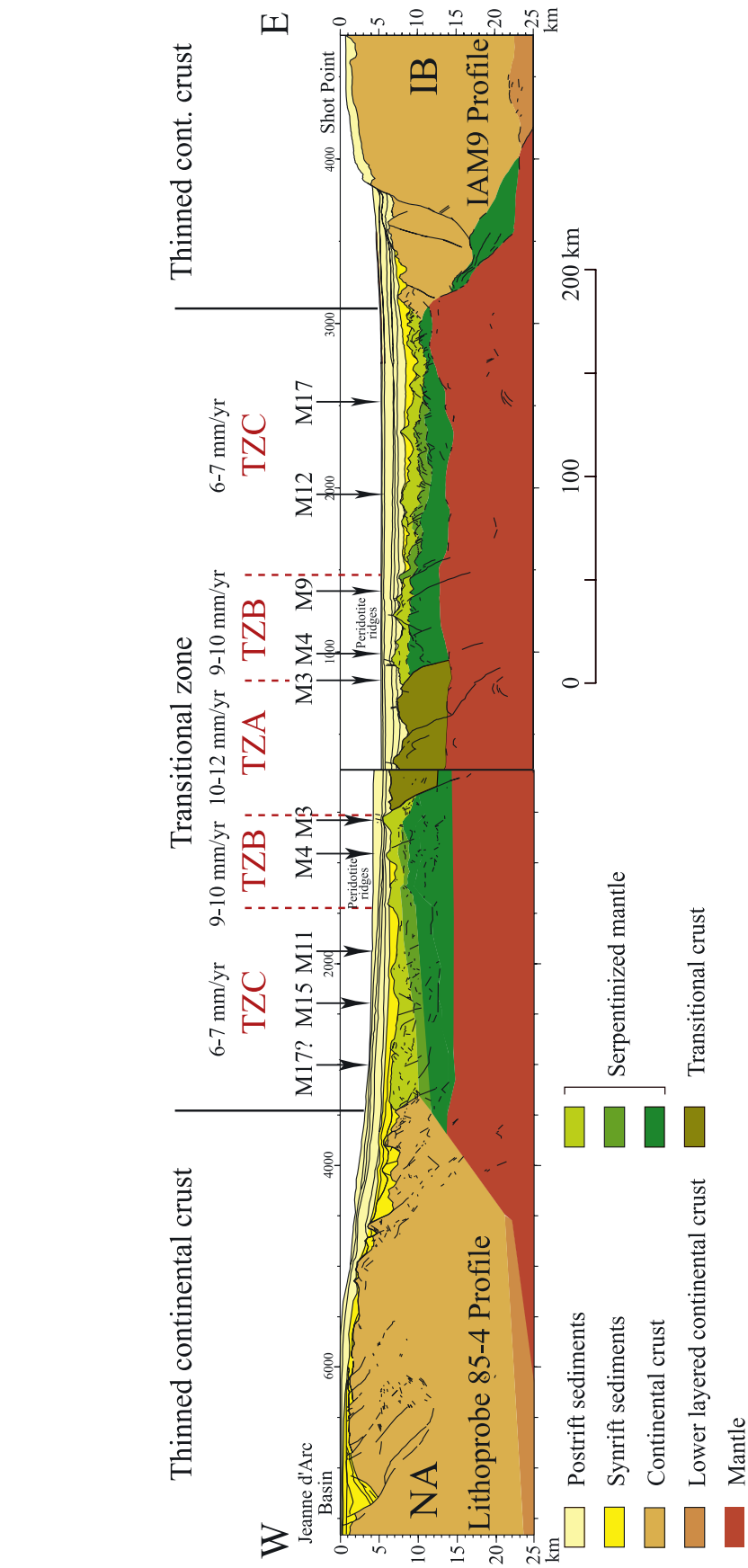

Figure 9. Line drawing of conjugate seismic profiles IAM9 and Lithoprobe 85-4 located in Figure 1 with the identification of main magnetic anomalies [*Srivastava et al.*, 2000], showing results of IAM9 refraction line [*Dean et al.*, 2000] complemented with land stations recordings providing velocity controls beneath the upper part of the Iberian continental margin (L. Matias, personal communication, 2001). Results of compiled refraction data acquired in the northern Newfoundland Basin [*Reid*, 1994; *Reid and Keen*, 1988] are extrapolated to Lithoprobe line 85-4. Preliminary refraction results of the *Erable* cruise concerning the eastern portion of the northern Newfoundland Basin are also shown (I. Reid, personal communication, 1992). Note that the magnetic lineations are approximately symmetrical. TZA, TZB, and TZC are portions of the transition zone with half extension/spreading rates above.

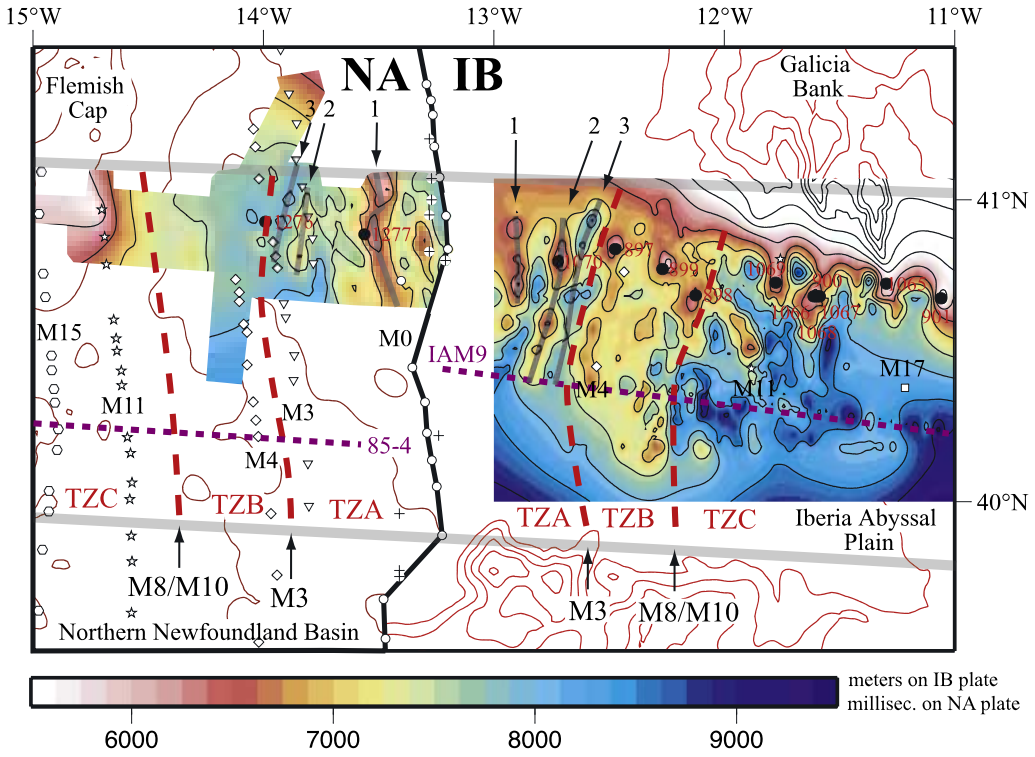

Figure 10. Basement depths on M0 reconstruction (parameters in Figure 1). On the Iberia (IB) side, depths in meters are from *Russell and Whitmarsh* [2003]. On the North America (NA) side, depths in milliseconds are from *Shillington et al.* [2004]. 1, 2, and 3 are parallel conjugate ridges or linear depressions located at the same distance from the M0 rift and consequently formed at the same time. The two light gray lines at about 40°N and 41°N latitude are the M25-M0 flow-lines of Figure 1 bounding the IAP/NNFB segment of conjugate margins. Dashed red lines are boundaries within the transition zone (TZA, TZB, and TZC). Black circles are ODP sites with their numbers given in red. Different symbols are magnetic picks of *Srivastava et al.* [2000].

depths in milliseconds obtained from gridded picks of pre-stack-time migration profiles [*Shillington et al.*, 2004]. Two subdomains appear in the transition zone:

[37] 1. A shallow basement domain located in TZA and TZB. Note that TZB on the NA side is deeper and smoother than its IB counterpart but it concerns the northernmost portion of the conjugate segment, which might belong to the northern adjacent Galicia/SE Flemish Cap segment. Ridges and basement troughs 1, 2, and 3 identified in the IAP and NNFB are parallel and located at the same distances of chron M0, which means that they have been created in a plate kinematic context. In TZAs and TZB on the IB side, the length of basement ridges is ~50 km.

[38] 2. A deep basement domain TZC on the IB side, whose boundary with the thinned continental domain is not obvious on the basement map. The ~20-km-long basement ridges and troughs are identified but the basement is smooth, particularly in the southern part of the IAP.

[39] The main change in basement depth occurs at the TZB/TZC boundary, which coincides with magnetic anomalies M8–M10 (late Valanginian–early Hauterivian, ~130 Ma). The TZA/TZB boundary coinciding with M3 (late Hauterivian, ~127 Ma) corresponds to a minor change in refraction velocities and gradients (Figure 9) and to the time at which peridotite ridges and associated magnetic lineations started to extend northward, west of the Galicia margin.

10. Oceanic Crust Proxies

[40] As half-spreading rates are comprised between 6 and 12 mm/yr in the IAP/NNFB transitional zones, it is worth looking at the properties of the slow and ultraslow spreading ridges, which can give some constraints on the nature of the IAP transitional crust and its mechanism of emplacement. We will discuss two representative examples of slow and ultraslow oceanic crust where high-resolution swath bathymetric, gravimetric and magnetic data have been collected: (1) the oceanic segments on each side of the central Atlantic 15°20′N FZ (12 mm/yr) and (2) the Southwest Indian Ridge (SWIR), close to the Rodriguez triple junction (7 mm/yr).

[41] Away from the 15°20′N FZ, the northern and southern segments (N3 and S3 in Figure 11a) display long abyssal hills with small spacing and fault throw (Figure 11d), well-lineated and high-amplitude magnetic anomalies (Figure 11b), and negative residual mantle Bouguer anomalies (Figure 11a) [*Fujiwara et al.*, 2003]. Crustal magnetization stripes (Figure 11c) display symmetric sea-floor spreading rates (e.g., for segment S3 in Figure 11e). Even though no exhumed mantle samples have yet been

collected in segments N3 and S3 (Figure 11d), it does not necessarily imply that serpentinized peridotites are absent in these segments. All these observations suggest a robust magmatic extension in these two segments.

[42] In contrast, the crust in the two ridge segments immediately north (N1 and N2) and south (S1 and S2) of the 15°20′N FZ is characterized by rugged and blocky topography, by low amplitude and discontinuous magnetization stripes and by high residual mantle Bouguer anomaly, implying thin crust over the 5-Ma considered period [*Fujiwara et al.*, 2003]. Crustal magnetization stripes (Figure 11c) display asymmetric seafloor spreading rates (e.g., for segments S1 and S2 in Figure 11e). Numerous samples of exhumed mantle have been collected in these segments though basaltic and gabbroic samples were also recovered (Figure 11d). Corrugated surfaces were found in the off-axis crust on both sides of ridge axes. All these observations suggest that the melt supply is minimum with little volcanism in these four segments. Despite the amagmatic character of these segments and the relative lack of volcanic rocks, magnetic lineations, though less clear than in magmatic segments, are clearly expressed but the anomalies may be partly caused by serpentinized peridotites. We conclude that, even if the spreading rate is constant in the whole area, melt supply varies between magmatic and amagmatic segments and is the main factor controlling the nature and morphology of the crust.

[43] In the SWIR area located immediately south of the Rodriguez triple junction, a continuous geophysical survey was performed between the fossil triple junction trajectories for the 0–30 Ma period of this ultraslow spreading system (7.2 mm/yr half-spreading rate) [*Cannat et al.*, 2006]. Here, the mean water depth is large ($\sim$ 4500 m), the crust is thin (3–4 km), and serpentinized peridotites were frequently dredged on ridge flanks [*Seyler et al.*, 2003]. Outside the rift valley, about 60% of the whole area corresponds to a volcanic seafloor with numerous cones and spreading perpendicular fault scarps in a similar manner than abyssal hills described at faster spreading seafloor [*Macdonald et al.*, 1996] and at more magmatically robust regions of ultraslow ridges [*Hosford et al.*, 2003; *Mendel et al.*, 2003]. The remaining 40% of the surface of the crust presents a deep smooth seafloor topography and numerous $\sim$20 $\times$ 20 km in size corrugated surfaces (2%). The smooth seafloor occurs in the form of broad ridges, 15–30 km long, 500–2000 m high, parallel to the rift valley. All dredges have sampled serpentinized peridotites, with or without gabbros and basalts [*Seyler et al.*, 2003]. Smooth terrains are specific of melt poor, ultraslow seafloor [*Cannat et al.*, 2006]. Linear magnetic lineations were identified in the whole area and have been interpreted as typical seafloor-spreading-type magnetic anomalies. The remarkable fits of conjugate magnetic lineations are a proof of the validity of kinematic solutions in the Indian Ocean. However, as 40% of the area consists of exhumed mantle, we suggest that magnetic lineations identified in the smooth terrains are linked to the serpentinization process rather than to the seafloor spreading process. This means that the crustal magnetization by serpentinization or magma emplacement in a seafloor spreading system gives the same result in terms of kinematic reconstructions.

[44] To summarize, volcanic and corrugated surfaces not only develop in ultraslow spreading regions as the Southwest Indian Ridge [*Cannat et al.*, 2006; *Hosford et al.*, 2003; *Mendel et al.*, 2003] and the Gakkel Ridge [*Dick et al.*, 2003; *Jokat et al.*, 2003; *Michael et al.*, 2003] but also at the slow spreading mid-Atlantic Ridge (e.g., at 15°20′N [*Fujiwara et al.*, 2003]) and at the fast spreading Australia-Antarctic Discordance (75 mm/yr) [*Okino et al.*, 2004]. By contrast, the smooth terrains, where exhumed mantle outcrops, appear to be specific of melt-poor, ultraslow seafloor and cover 40% of the surface of the Southwest Indian Ridge domain N-E of 61°E longitude. Consequently, if the melt supply, which is linked to the thermal state of the lithosphere, is the main controlling factor on the morphology and composition of the newly emplaced seafloor, the extension/spreading rate is an important factor only for ultraslow spreading crust where 40% of the surface corresponds to smooth seafloor that forms at minimal melt supply.

[45] Comparing the magnetic records of slow and ultraslow spreading regions with those in the IAP and NNFB, we are now confident that in the transitional zones of the IAP and northern Newfoundland Basin, the almost symmetrical magnetic anomalies of the M-sequence are not basically generated by volcanic rocks but rather by the serpentinized exhumed mantle with a small amount of gabbro and basalt. Modeling of magnetic anomalies created by igneous crust or serpentinized mantle gives similar results in term of basement age, even if the amplitude of magnetic anomalies and crustal magnetization are highly variable. To illustrate this, we will refer to the seismic section across the IAP/NNFB conjugate segments (Figure 9) and the reconstruction of basement depths at chron M0 (Figure 10).

11. Model of Formation of Transitional Zones

[46] Understanding the mode of formation of the transitional crust at the base of continental margins is a difficult challenge because of limited sampling and the presence of thick postrift sediments. However, the IAP/NNFB drilling transect as well as oceanic slow and ultraslow proxies provide a unique opportunity to improve our understanding of the fundamental processes involved in the formation of

Figure 11. Geophysical data on each side of the 15°20′N fracture zone (FZ) [*Fujiwara et al.*, 2003]. Dashed lines are segment boundaries. (a) Mantle Bouguer gravity anomalies contoured at 5 mGal intervals. (b) Magnetic anomaly map. Thin and thick lines mark 25 and 100 nT contours, respectively. (c) Crustal magnetization calculated from magnetic data. Contour intervals are every 2 A/m. Red circles mark peaks of normal polarity anomalies along ship tracks, and blue circles mark peaks of reversed polarity anomalies. (d) Detailed bathymetry and rock samples south of the 15°20′N FZ; red dots: basalt; blue squares: gabbro; green dots: ultramafic. Thin and thick contour lines are at 100 m and 1000 m intervals, respectively. (e) Full-spreading rates on the left and half-spreading rates on the right.

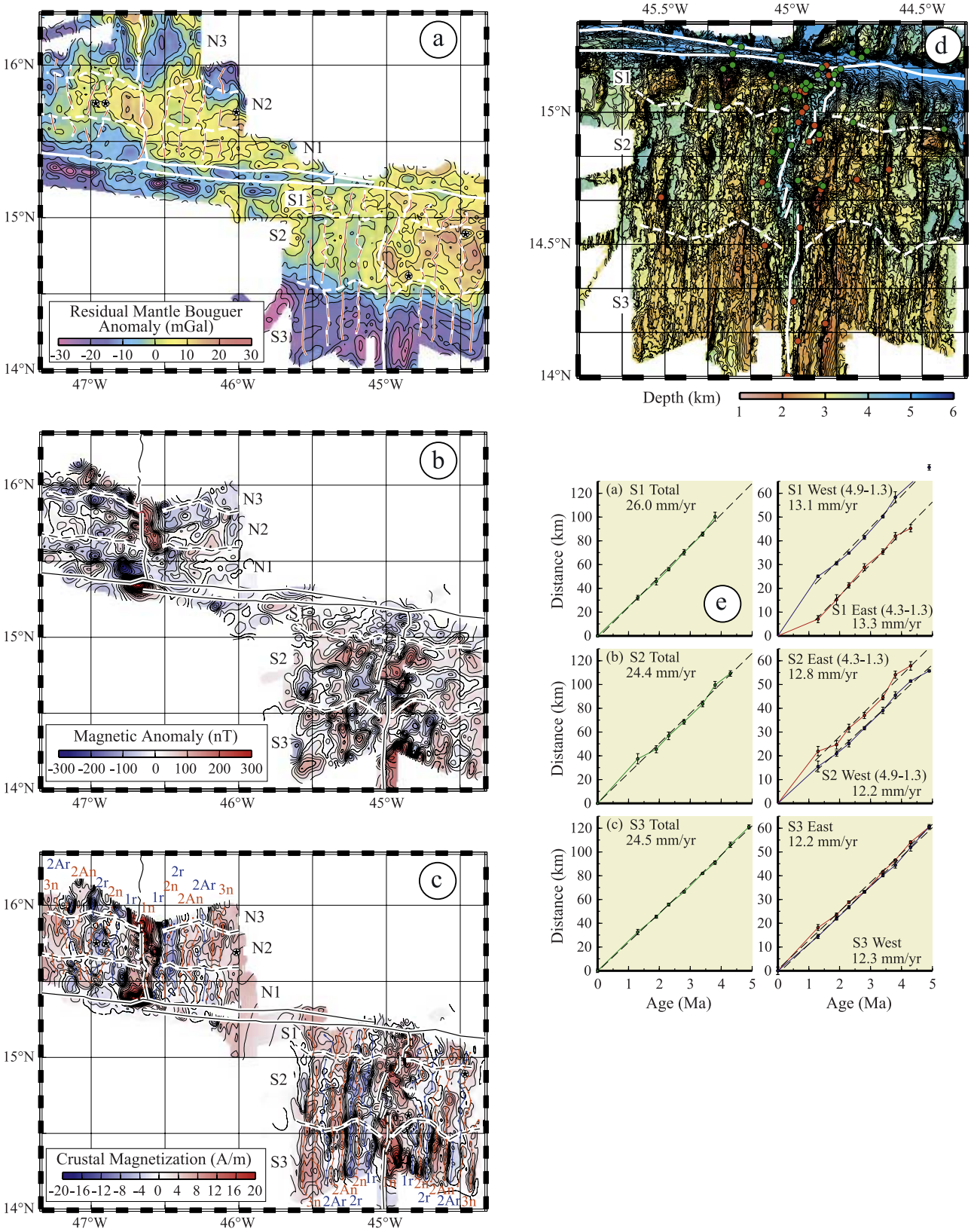
a
N3
N2
N1
S1
S2
S3
Residual Mantle Bouguer Anomaly (mGal)
-30 -20 -10 0 10 20 30
16°N
15°N
14°N
47°W
46°W
45°W
b
Magnetic Anomaly (nT)
-300 -200 -100 0 100 200 300
c
Crustal Magnetization (A/m)
-20 -16 -12 -8 -4 0 4 8 12 16 20
d
45.5°W
45°W
44.5°W
14.5°N
Depth (km)
1 2 3 4 5 6
e
(a) S1 Total
26.0 mm/yr
S1 West (4.9-1.3)
13.1 mm/yr
S1 East (4.3-1.3)
13.3 mm/yr
(b) S2 Total
24.4 mm/yr
S2 East (4.3-1.3)
12.8 mm/yr
S2 West (4.9-1.3)
12.2 mm/yr
(c) S3 Total
24.5 mm/yr
S3 East
12.2 mm/yr
S3 West
12.3 mm/yr
Distance (km)
Age (Ma)

Figure 11

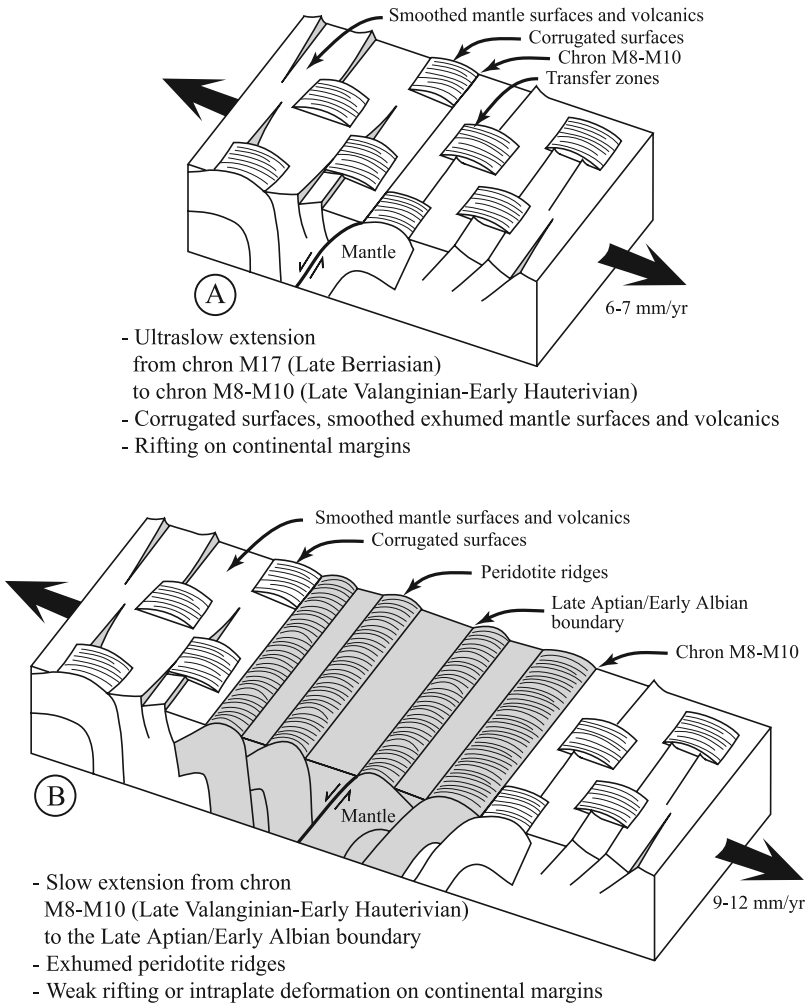

Figure 12. Model of formation of the transitional crust in two stages: (a) Formation from chron M17 (early Berriasian) to chrons M8-M10 (late Valanginian–early Hauterivian) of the deep smooth domain with corrugated surfaces characteristic of melt-poor ultraslow seafloor similar in size to those of the Southwest Indian Ridge (SWIR) area. (b) Formation from chrons M8-M10 to the Aptian/Albian boundary of the peridotite ridges domain as for the 15°20'N FZ amagmatic segments (in gray).

transitional crust. On the basis of geophysical and drilling results, we propose a model (Figure 12), which synthesizes the formation of the transitional crust for this type of nonvolcanic continental margins. We consider that the transitional crust is mainly formed of exhumed mantle with a variable amount of gabbro and basalt depending on the thermal state of the lithosphere, mantle composition and extension rate. Slow and ultraslow midoceanic ridge analogs as well as field examples in the Alps, though knowledge about them is still incomplete concerning the ultraslow spreading segments, provide useful complementary guides.

[47] We compare the formation of the oldest deep portions of the transitional IAP and NNFB crusts (TZCs) with the formation of the ultraslow spreading ridges [*Cannat et al.*, 2006; *Dick et al.*, 2003] (Figure 12). Basement depths and half extensional rates are similar (6–7 mm/yr in TZCs and 7 mm/yr in the SWIR area). By analogy, we postulate the presence of limited size corrugated surfaces (~20 × 20 km) and smooth surfaces (~40% of the whole surface), even though it is impossible to prove their presence below sediments with the present-day available drilling or geophysical tools. The rest of the transitional crust (~60%) might be formed by volcanic crust. The gross symmetry of magnetic anomalies of the M-sequence might be accounted by the extension resulting in the formation of smooth and corrugated surfaces, each mullion occurring at a given time on one side of the rift axis and giving flipped polarity over periods of a few millions years.

[48] The youngest part of the transitional zone (TZAs and TZBs, Figures 9 and 10) is shallow and composed of ~50-km-long symmetrical peridotite ridges (Figure 10). This domain is similar to slow spreading amagmatic segments N1, N2 and S1, S2 on each side of the 15°20′N FZ (Figure 11). Half extension rates are similar (9–12 mm/yr for TZA and TZB and 12 mm/yr for the 15°20′N FZ). As half-spreading rates on each side of rift axes are slightly asymmetrical for segments N2, N1, S1 and S2 (Figure 11e) [*Fujiwara et al.*, 2003], we suggest that exhumed mantle ridges in the transition zones might be emplaced by a flip-

flop mechanism resulting in a nonsimultaneous emplacement of opposite dipping ridges [*Cannat et al.*, 2004] (Figure 12).

12. Other Examples of Transitional Crust Proxies

[49] Several examples suggest that some magnetic lineations initially defined in the so-called oceanic domain belong in fact to transitional domains. The first example concerns the Labrador Sea where *Srivastava and Roest* [1995] find low-amplitude magnetic anomalies C31 to C33 lying over regions which might be underlain by serpentinized mantle [*Chian et al.*, 1995a, 1995b; *Keen et al.*, 1994]. The formation of these margins has also been the subject of a similar controversy [e.g., *Srivastava and Roest*, 1995; *Chalmers and Laursen*, 1995] that for the Newfoundland-Iberia rift. *Srivastava and Roest* [1995] interpreted anomalies across these margins to have been formed at an ultraslow spreading half-rate of 5.8 mm/yr whereas *Chalmers and Laursen* [1995] regard them as igneous intrusions within the thinned continental crust. The thinness of the serpentinized crust and the low amplitudes of anomalies C31 to C33 across the margins are similar to our observations across the IAP margin and it suggests that these anomalies are caused by serpentinized crust and not only by volcanics formed at these ultraslow spreading rates as previously interpreted [*Srivastava and Roest*, 1995]. Seaward, magnetic anomalies C29 to C21 are typical seafloor spreading anomalies formed at half-spreading rate of 10 to 15 mm/yr [*Srivastava and Roest*, 1995] and present the same characteristics than magnetic anomalies younger than the Aptian/Albian boundary along the IAP/NNFB transect.

[50] The second example concerns the south Australia-Antarctica conjugate margins. *Tikku and Cande* [1999] have identified magnetic lineations C18 to C34 on both sides of the ocean as well as the Quiet Magnetic Zone Boundary. Their proposed kinematic reconstructions for anomalies C32, C33, C34 and the Quiet Magnetic Zone Boundary are very convincing. Anomaly C34, for example, is a well-defined anomaly extending over 1200 km on the two conjugate margins and larger than 50 nT in amplitude. On the basis of MCS profiles acquired on both margins, magnetic lineations C34 are always located inside the transitional zones defined by *Sayers et al.* [2001], *Direen et al.* [2007] and *Beslier et al.* [2004] on the southern Australia margin and by *Colwell et al.* [2007] on the Antarctica margin. More precisely, the seaward boundary of the transition zone approximately follows magnetic lineation C33 in the central Great Australia Bight [*Sayers et al.*, 2001] and continues westward in the southern part of the Diamantina Zone [*Beslier et al.*, 2004; *Direen et al.*, 2007], close to the location of magnetic lineation C21 where the spreading rate suddenly increased from 6.5 to 10 mm/yr. Dredge samples [*Beslier et al.*, 2004; *Borissova*, 2002] obtained in the smooth transitional domain located between the Naturaliste Plateau and the Diamantina Zone contain mantle rocks intruded by gabbros. On the basis of MCS data, the transitional domain offshore Wilkes Land and Terre Adélie extends along an irregular boundary, which undulates between magnetic lineations C33 and C21 [*Colwell et al.*, 2007]. Seismic arguments used to delineate the seaward boundaries of transitional domains seem to be convincing. If these observations are correct, the seaward boundary of the transition zone does not follow the same isochron all along the 1200 km of continental margins, suggesting that the end of the rifting phase is diachronous from one segment of continental margin to another one.

[51] All these observations suggest mantle exhumation during rifting, before the onset of seafloor spreading. These two examples illustrate that some magnetic anomalies located within the transitional domains are not typical seafloor spreading anomalies even if they are symmetrical on both sides of the ocean [*Srivastava and Roest*, 1995; *Tikku and Cande*, 1999]. The presence of exhumed mantle allows for the possibility that magnetic anomalies are the consequence of mantle serpentinization during exhumation. The area of linear peridotite ridges, which forms the Diamantina Zone, looks like the peridotite ridges of the IAP/NNFB transect (TZA and TZB), both in terms of width and nature of crust. Even if ages of these continental margins are different, some common processes of formation may be involved.

13. Continental Breakup

[52] The notion of breakup or separation of continents and subsequent formation of oceanic crust was defined a long time ago with the arrival of plate tectonics. At that time, the breakup unconformity, marked by broad well-developed unconformity on seismic records, separated the synrift and postrift sediments and corresponded to the end of extensional processes on continental margins (rifting episode). Since the early 1970s, on the basis of structural analyses and from dredging, coring, and drilling results, the breakup unconformities in the northern Bay of Biscay, Galicia, and IAP margins have been dated late Aptian-early Albian [*Groupe Galice*, 1979; *Montadert et al.*, 1979]. It implied that the onset of oceanic crust started in these regions at the Aptian/Albian boundary. However, we have identified in the IAP a large transitional zone, younger than the Aptian/Albian boundary, consisting of exhumed mantle lying between the thinned continental and the true oceanic crust and showing the same characteristics than slow and ultraslow spreading crusts. This raises the question about the correspondence of the breakup unconformity with the onset of oceanic crust.

[53] The J anomaly (M1–M3) was recognized a long time ago west of Iberia [e.g., *Rabinowitz et al.*, 1978], and older magnetic anomalies M4 to M17 [*Srivastava et al.*, 2000] more recently. Similarly, magnetic anomalies of the M-sequence (M0–M3) were only recognized in the Bay of Biscay in 2004 [*Sibuet et al.*, 2004b]. As previously seen, the IAP and northern Bay of Biscay transition zones bear the characteristics of ultraslow and slow oceanic crust. Half extension/spreading rates continuously increase from ultraslow rates (6–7 mm/yr) on the continent side of transition zones to slow rates (9–12 mm/yr) on their ocean side.

[54] The Late Jurassic-Aptian/Albian rifting episode can be divided into two main episodes: (1) From Late Jurassic to early Berriasian, extension resulted in thinning of the continental crust. This first tensional episode primarily affected the Lusitanian and Galicia Interior basins, and it was probably associated with final extension of continental crust and initial exhumation of lithospheric mantle south of

Galicia Bank [*Tucholke et al.*, 2007]. (2) Then, from Berriasian to the Aptian/Albian boundary, the transition zone was built mostly by mantle exhumation in a way similar to the production of ultraslow and slow spreading oceanic crusts. This second tensional episode was not only focused in the transition zone but also in the most distal part of the margin. Within the IAP thinned continental crust, deformation occurred as short tensional episodes, in particular near the Berriasian/Valanginian and Hauterivian/Barremian boundaries [*Tucholke et al.*, 2007]. Several examples of intraplate extension within the transitional zone itself were also identified by *Tucholke et al.* [2007], suggesting that tensile stress concentrated in weak zones such as serpentinized areas. *Tucholke et al.* [2007] also proposed that the rising asthenosphere finally breached near the Aptian/Albian boundary, leading to localized magmatic seafloor spreading. Simultaneously, intraplate tensile stress was released, causing local and regional deformation that stimulated mass wasting resulting in basin-wide deposition of reflective sedimentary layers that define the Aptian/Albian unconformity [*Tucholke et al.*, 2007]. This unconformity is considered as the last significant tensional event at the origin of significant mass wasting and turbidity currents responsible of the strong acoustic character of this unconformity.

[55] The above interpretation questions the concept of the breakup unconformity and it is impossible to favor one of the following interpretations: (1) If several tensional episodes affected the thinned continental crust until the Aptian/Albian boundary, it means that rifting is still active during mantle exhumation but at a smaller rate as part of the extension is absorbed by the mantle exhumation process as well as by intraplate deformation within the transition zone. (2) Mantle exhumation absorbed most of the available extension and the amount of extension absorbed by the thinned continental crust before the breakup unconformity is minor and considered as intraplate deformation. In this hypothesis, the breakup unconformity might be much older than late Aptian-early Albian and might be associated with the onset of mantle exhumation dated close to late Berriasian [*Tucholke et al.*, 2007] or slightly younger than the oldest identified magnetic anomaly (M17, early Berriasian).

[56] More generally, there is now an open discussion concerning the age of the end of the main rifting phase observed on continental margins [e.g., *Péron-Pinvidic et al.*, 2007; *Sibuet et al.*, 2004a], which might be associated with a transient thermal uplift caused by the rise of asthenosphere after the emplacement of the transitional crust [*Reston and Morgan*, 2004], a relaxation of tensional forces [*Bowling and Harry*, 2001] and a resulting relative compression phase on continental margins [*Tucholke et al.*, 2007], or a change in the nature of the crust from amagmatic to magmatic.

14. Conclusions

[57] In this paper, we have shown that

[58] 1. Magnetic anomalies identified within the transitional zones located between Iberia and North America are symmetrical. Their amplitudes are reduced compared with the magnetic anomalies of the M-sequence recorded in the central Atlantic Ocean.

[59] 2. Paleomagnetic data at ODP sites are consistent with two successive episodes of mantle serpentinization: a first one during which a strong component of magnetization was acquired, followed by a second episode of serpentinization occurring at the contact to cold seawater, and which only affects the upper tens of meters.

[60] 3. During mantle exhumation, magnetite grains have recorded the ambient magnetic field at crustal levels, during mantle cooling. As soon as the serpentinized mantle was exhumed or close to the seafloor, the upper several tens of meters of serpentinized peridotite started to be altered by seawater (Fischer-Tropsch reaction).

[61] 4. Ages of mantle exhumation at ODP sites 1068, 1070 and 1277 are similar to ages determined from magnetic lineations supposed to be created by seafloor spreading.

[62] 5. The inversion of power spectra and a combined inversion for the structural index and the source location by using the Euler deconvolution show that magnetic sources are N-S trending horizontal cylinders located within the highly serpentinized basement to a depth of 2–3 km. It is unlikely that the observed magnetic anomalies were produced by lower crustal synextensional intrusions located about 6–8 km beneath the top of the basement.

[63] 6. The serpentinization process was able to produce magnetic lineations formed in a similar way as in the basaltic oceanic crust formed at midocean ridges, with the difference that the resulting field might be much weaker and more variable in space.

[64] 7. Within transition zones, sequences of magnetic anomalies are mainly produced by the serpentinization process and can provide information concerning the timing of crust emplacement but not on the nature of the crust (oceanic crust versus exhumed mantle or a combination of both).

[65] 8. A comparison with slow and ultraslow midoceanic spreading ridges shows that the transition zone was formed by ultraslow extension from M17 (early Berriasian) to M8/M10 (late Valanginian-early Hauterivian) and by slow extension from Hauterivian to the late Aptian-early Albian boundary.

[66] 9. After thinning of the continental crust, the transition zone was created as ultraslow and slow spreading crusts. Simultaneously, rifting continued on continental margins as discrete tensional events related to changes in extension rates.

[67] 10. Transitional zones with similar characteristics exist in the Labrador Sea and between the Australia and Antarctica for example. We have now a way to date the emplacement of mantle basement of transition zones and to provide kinematic reconstructions during rifting of continental margins.

[68] **Acknowledgments.** The GMT software package was used to make Figures 1, 2, 4, 9, and 10 [*Wessel and Smith*, 1991]. We thank R.B. Whitmarsh and D. Shillington for making available their basement grids in the Iberia Abyssal Plain and Newfoundland Basin, respectively, and L. Matias for refraction velocities beneath the Iberian shelf in advance of publication. We also thank W.-B. Doo and H.-K. Hsu for operating their new Euler deconvolution method on the TOBI91 deep-tow profile in order to calculate simultaneously the structural index and the depth of magnetic sources. We acknowledge numerous fruitful discussions with P. Bascou, S. Cande, N.G. Direen, L. Gernigon, S.-K. Hsu, T. Minshull, W. Roest, D. Sawyer, X. Zhao, and particularly B. Tucholke, cochief scientist during ODP leg 210 with whom we intensively discussed the problem of breakup

of the Newfoundland-Iberia rift. We also acknowledge the careful and very constructive reviews of A. Dijkstra and M. Enachescu. This research used data provided by the Ocean Drilling Program (ODP). ODP is sponsored by the U.S. National Science Foundation and participating countries under management of Joint Oceanographic Institutions (JOI).

References

Beard, J. S., P. D. Fullagar, and A. Krisha Sinha (2003), Gabbroic pegmatite intrusions, Iberia Abyssal Plain, ODP leg 173, site 1070: Magmatism during a transition from non-volcanic rifting to sea-floor spreading, *J. Petrol.*, *43*, 885–905.

Beslier, M.-O., et al. (2004), Une large transition océan-continent en pied de marge sud-ouest australienne: Premiers résultats de la campagne MARGAU/MD110, *Bull. Soc. Geol. Fr.*, *175*, 629–641.

Bill, M., L. O'Dogherty, J. Guex, P. O. Baumgartner, and H. Masson (2001), Radiolarite ages in Alpine-Mediterranean ophiolites: Constraints on the oceanic spreading and the Tethys-Atlantic connection, *Geol. Soc. Am. Bull.*, *113*, 129–143.

Bina, M. M., and B. Henry (1990), Magnetic properties, opaque mineralogy and magnetic anisotropies of serpentinized peridotites from ODP hole 670A near the mid-Atlantic Ridge, *Phys. Earth Planet. Inter.*, *65*, 88–103.

Borissova, I. (2002), Geological framework of the Naturaliste Plateau, in *Geosci. Aust. Rec. 2002/020*, vol. 44, 21 pp., Geosci. Aust., Canberra, Australia.

Bowling, J. C., and D. L. Harry (2001), Geodynamic models of continental extension and the formation of non-volcanic rifted margins, in *Non-Volcanic Rifting of Continental Margins: A Comparison of Evidence From Land and Sea*, edited by R. C. L. Wilson et al., *Geol. Soc. Spec. Publ.*, *187*, 511–536.

Cannat, M., D. Sauter, E. Ruellan, K. Okino, V. Mendel, J. Escartin, V. Combier, and M. Baala (2004), Tectonique extensive et morphologie du plancher océanique d'une dorsale ultra-lente: Un cas extrême de dénudation du manteau, paper presented at Réunion Sciences de la Terre, Soc. Geol. de France, Strasbourg, 20–25 Sept.

Cannat, M., D. Sauter, V. Mendel, E. Ruellan, K. Okino, J. Escartin, V. Combier, and M. Baala (2006), Modes of seafloor generation at a melt-poor ultra-slow spreading ridge, *Geology*, *34*, 605–608.

Chalmers, J. A., and K. H. Laursen (1995), Labrador Sea: The extent of continental and oceanic crust and the timing of the onset of seafloor spreading, *Mar. Pet. Geol.*, *12*, 205–217.

Chian, D., C. E. Keen, I. D. Reid, and K. E. Louden (1995a), Evolution of nonvolcanic rifted margins: New results from the conjugate margins of the Labrador Sea, *Geology*, *23*, 589–592.

Chian, D., K. E. Louden, and I. D. Reid (1995b), Crustal structure of the Labrador Sea conjugate margins and implications for the formation of nonvolcanic continental margins, *J. Geophys. Res.*, *100*, 24,239–24,254.

Chian, D., K. E. Louden, T. A. Minshull, and R. B. Whitmarsh (1999), Deep structure of the ocean-continent transition in the southern Iberia Abyssal Plain from seismic refraction profiles: 1. Ocean Drilling Program (legs 149 and 173) transect, *J. Geophys. Res.*, *104*, 7443–7462.

Christensen, N. I. (1978), Ophiolites, seismic velocities and oceanic crustal structure, *Tectonophysics*, *47*, 131–157.

Colwell, J. B., H. M. J. Stagg, N. G. Direen, G. Bernardel, and J. Borissova (2007), The structure of the continental margin off Wilkes Land and Terre Adélie, East Antartica, in *Imaging, Mapping and Modelling Continental Lithosphere Extension and Breakup*, edited by G. Karner, G. Manatschal, and L. M. Pinheiro, *Geol. Soc. Spec. Publ.*, *282*, in press.

Cornen, G., J. Girardeau, and C. Monnier (1999), Basalts, underplated gabbros, and pyroxenites record the rifting process of the west Iberian margin, *Mineral. Petrol.*, *67*, 111–142.

Dean, S. M., T. A. Minshull, R. B. Whitmarsh, and K. E. Louden (2000), Deep structure of the ocean-continent transition in the southern Iberia Abyssal Plain from seismic refraction profiles: The IAM-9 transect at 40°20′N, *J. Geophys. Res.*, *105*, 5859–5886.

Dick, H. J. B., J. Lin, and H. Schouten (2003), An ultraslow-spreading class of ocean ridge, *Nature*, *426*, 405–412.

Direen, N. G., J. Borissova, H. M. J. Stagg, J. B. Colwell, and P. A. Symonds (2007), Nature of the continent-ocean transition zone along the southern Australian continental margin: A comparison of the Naturaliste Plateau, south-western Australia, and the central Great Australian Bight sectors, in *Imaging, Mapping and Modelling Continental Lithosphere Extension and Breakup*, edited by G. Karner, G. Manatschal, and L. M. Pinheiro, *Geol. Soc. Spec. Publ.*, *282*, in press.

Dunlop, D. J., and M. Prévot (1982), Magnetic properties and opaque mineralogy of drilled submarine intrusive rocks, *Geophys. J. R. Astron. Soc.*, *69*, 763–802.

Féraud, D., M.-O. Beslier, and G. Cornen (1996), $^{40}Ar/^{39}Ar$ dating of gabbros from the ocean-continent transition of the western Iberia margin: Preliminary results, *Proc. Ocean Drill. Program Sci. Res.*, *149*, 489–495.

Fiet, N., X. Quidelleur, O. Parize, L. G. Bulot, and P-Y. Gilot (2006), Lower Cretaceous stage durations combining radiometric data and orbital chronology: Towards a more stable relative time scale?, *Earth Planet. Sci. Lett.*, *246*, 407–417.

Froitzheim, N., and G. P. Eberli (1990), Extensional detachment faulting in the evolution of a Tethys passive continental margin, eastern Alps, Switzerland, *Geol. Soc. Am. Bull.*, *102*, 1297–1308.

Frueh-Green, G. L., C. Boschi, D. S. Kelley, J. A. Connolly, and M. O. Schrenk (2002), The role of serpentinization in metasomatism, carbonate precipitation and microbial activity: Stable isotope constraints from the Lost City Vent Field (MAR 30°N), *Eos Trans. AGU*, *83*(47), Fall Meet. Suppl., Abstract 1289.

Fujiwara, T., J. Lin, T. Matsumoto, P. B. Kelemen, B. E. Tucholke, and J. F. Casey (2003), Crustal evolution of the mid-Atlantic Ridge near the Fifteen-Twenty fracture zone in the last 5 Ma, *Geochem. Geophys. Geosyst.*, *4*(3), 1024, doi:10.1029/2002GC000364.

Gradstein, F. M., F. P. Agterberg, J. G. Ogg, J. Hardenbol, P. van Veen, J. Thierry, and Z. Huang (1995), A Triassic, Jurassic and Cretaceous time scale, in *Geochronology, Time Scales and Global Stratigraphic Correlation*, *Spec. Publ. SEPM Soc. Sediment. Geol.*, *54*, 95–126.

Gradstein, F. M., J. G. Ogg, and A. G. Smith (2004), *A Geologic Time Scale 2004*, 589 pp., Cambridge Univ. Press, Cambridge, U. K.

Groupe Galice (1979), The continental margin off Galicia and Portugal: Acoustical stratigraphy, dredge stratigraphy and structural evolution, in *Initial Reports of the Deep Sea Drilling Project*, edited by J.-C. Sibuet et al., pp. 633–662, U.S. Gov. Print. Off., Washington, D. C.

Horen, H., and G. Dubuisson (1995), Rôle de l'hydrothermalisme sur les propriétés magnétiques d'une lithosphère océanique formée à l'axe d'une ride lente: L'ophiolite de Xigaze, *C. R. Acad. Sci. Paris*, *312*, 1095–1102.

Horen, H., M. Zamora, and G. Dubuisson (1996), Seismic waves velocities and anisotropy in serpentinized peidotites from Xigaze ophiolite: Abundance of serpentine at slow spreading ridges, *Geophys. Res. Lett.*, *23*, 9–12.

Hosford, A., M. A. Tivey, T. Matsumoto, H. J. B. Dick, H. Schouten, and H. Kinoshita (2003), Crustal magnetization and accretion at the Southwest Indian Ridge near the Atlantis II fracture zone, 0–25 Ma., *J. Geophys. Res.*, *108*(B3), 2169, doi:10.1029/2001JB000604.

Hsu, S.-K. (2002), Imaging magnetic sources using Euler's equation, *Geophys. Prospect.*, *50*, 15–25.

Hsu, S.-K., D. Coppens, and C.-T. Shyu (1998), Depth to magnetic source using the generalized analytic signal, *Geophysics*, *63*, 1947–1957.

Jagoutz, O., O. Müntener, G. Manatschal, D. Rubato, G. Péron-Pinvidic, B. D. Turrin, and I. M. Villa (2007), The rift-to-drift transition in the southern North Atlantic: A stuttering start of the MORB engine?, *Geology*, in press.

Jokat, W., O. Ritzmann, M. C. Schmidt-Aursch, S. Drachev, S. Gauger, and J. Snow (2003), Geophysical evidence for reduced melt production on the Arctic ultraslow Gakkel mid-ocean ridge, *Nature*, *423*, 962–965.

Keen, C. E., and B. de Voogd (1988), The continent-ocean boundary at the rifted margin off eastern Canada: New results from deep seismic reflection studies, *Tectonics*, *7*, 107–124.

Keen, C. E., P. Potter, and S. Srivastava (1994), Deep seismic reflection data across the conjugate margins of the Labrador Sea, *Can. J. Earth Sci.*, *31*, 192–205.

Kent, D. V., and F. M. Gradstein (1986), A Jurassic to recent chronology, in *The Geology of North America,* vol. M, *The Western North Atlantic Region*, edited by P. R. Vogt and B. E. Tucholke, pp. 45–50, Geol. Soc. of Am., Boulder, Colo.

Keslo, P. R., C. Richter, and J. E. Pariso (1996), Rock magnetic properties, magnetic mineralogy and paleomagnetism of peridotite from site 895, Hess Deep, in *Proc. Ocean Drill. Program Sci. Results*, *147*, 405–413.

Kuhnt, W., and E. Urquhart (2001), Tethyan flysch-type benthic foraminiferal assemblages in the North Atlantic-Cretaceous to Paleogene deep water agglutinated foraminifers from the Iberia Abyssal Plain (ODP leg 173), *Rev. Micropaleontol.*, *44*(1), 27–59.

Lemoine, M., P. Tricart, and G. Boillot (1987), Ultramafic and gabbroic ocean floor of the Ligurian Tethys (Alps, Corsica, Apennines): In search of a genetic model, *Geology*, *15*, 622–625.

Lombardo, B., D. Rubatto, and D. Castelli (2002), Ion microprobe U-Pb dating of zircon from a Monviso metaplagiogranite: Implications for the evolution of the Piedmont-Liguria Tethys in the western Alps, *Ofioliti*, *27*, 109–117.

Macdonald, K. E., P. J. Fox, R. T. Alexander, R. A. Pockalny, and P. Gente (1996), Volcanic growth faults and the origin of Pacific abyssal hills, *Nature*, *380*, 125–129.

Manatschal, G. (2004), New models for evolution of magma-poor rifted margins based on a review of data and concepts from west Iberia and the Alps, *Int. J. Earth Sci.*, *93*, 432–466.

Manatschal, G., and P. Nivergelt (1997), A continent-ocean transition recorded in the Err and Platta nappes (eastern Switzerland), *Eclogae Geol. Helv.*, *90*, 3–27.

Manatschal, G., D. Marquer, and G. L. Frueh-Green (2000), Channelized fluid flow and mass transfer along a rift-related detachment fault (eastern Alps, southeastern Switzerland), *Geol. Soc. Am. Bull.*, *112*, 21–33.

Manatschal, G., N. Froitzeim, M. Rubenach, and B. D. Turrin (2001), The role of detachment faulting in the formation of an ocean-continent transition: Insights from the Iberia Abyssal Plain, in *Non-Volcanic Rifting of Continental Margins: A Comparison of Evidence From Land and Sea*, *Geol. Soc. Spec. Publ.*, *187*, 405–428.

Mendel, V., D. Sauter, C. Rommevaux-Jestin, P. Patriat, and E. Lefebvre (2003), Magmato-tectonic cyclicity at the ultra-slow spreading Southwest Indian Ridge: Evidence from variations of axial volcanic ridge morphology and abyssal hills pattern, *Geochem. Geophys. Geosyst.*, *4*(5), 9102, doi:10.1029/2002GC000417.

Michael, P. J., et al. (2003), Magmatic and amagmatic seafloor generation at ultraslow-spreading Gakkel Ridge, Arctic Ocean, *Nature*, *423*, 956–961.

Miles, P., J. Verhoef, and R. Macnab (1996), Compilation of magnetic anomaly chart west of Iberia, in *Proc. Ocean Drill. Program Sci. Results, 149*, 659–663.

Miller, D. J., and N. I. Christensen (1997), Seismic velocities of lower crustal and upper mantle rocks from the slow spreading mid-Atlantic Ridge, south of the Kane transform zone (MARK), in *Proc. Ocean Drill. Program Sci. Results, 153,* 437–454.

Montadert, L., O. de Charpal, D. Roberts, P. Guennoc, and J.-C. Sibuet (1979), Northeast Atlantic passive continental margins: Rifting and subsidence processes, in *Deep Drilling Results in the Atlantic Ocean: Continental Margins and Paleoenvironment, Maurice Ewing Ser.*, vol. 3, edited by M. Talwani, W. Hay, and W. B.F. Ryan, pp. 154–186, AGU, Washington, D. C.

Nazarova, K. A. (1994), Serpentinized peridotites as a possible source for oceanic magnetic anomalies, *Mar. Geophys. Res.*, *16*, 455–462.

Okino, K., K. Matsuda, D. M. Christie, Y. Nogi, and K. Koizumi (2004), Development of oceanic detachment and asymmetric spreading at the Australian-Antarctic Discordance, *Geochem. Geophys. Geosyst.*, *5*, Q12012, doi:10.1029/2004GC000793.

Oufi, O., M. Cannat, and H. Horen (2002), Magnetic properties of variably serpentinized abyssal peridotites, *J. Geophys. Res.*, *107*(B5), 2095, doi:10.1029/2001JB000549.

Parker, R. L., and L. P. Huestis (1974), The inversion of magnetic anomalies in the presence of topography, *J. Geophys. Res.*, *79*, 1587–1593.

Péron-Pinvidic, G., G. Manatschal, T. A. Minshull, and D. S. Sawyer (2007), Tectonosedimentary evolution of the deep Iberia-Newfoundland margin: Evidence for a complex breakup history, *Tectonics*, *26*, TC2011, doi:10.1029/2006TC001970.

Peters, T., and A. Stettler (1987), Time, physical-chemical conditions, mode of emplacement and geological setting of the total peridotite in the eastern Swiss Alps, *Schweiz Mineral. Petrogr. Mitt.*, *67*, 285–294.

Pickup, S. L.B., R. B. Whitmarsh, C. M.R. Fowler, and T. J. Reston (1996), Insight into the nature of the ocean-continent transition off west Iberia from a deep multichannel seismic reflection profile, *Geology*, *24*, 1079–1082.

Rabinowitz, P. D., S. C. Cande, and D. E. Hayes (1978), Grand Banks and J-Anomaly Ridge, *Science*, *202*, 71–73.

Reid, I. D. (1994), Crustal structure of a nonvolcanic rifted margin east of Newfoundland, *J. Geophys. Res.*, *99*, 15,161–15,180.

Reid, I. D., and C. E. Keen (1988), Upper crustal structure derived from seismic refraction experiments: Grand Banks of eastern Canada, *Bull. Can. Pet. Geol.*, *36*, 388–396.

Reston, T. J., and J. P. Morgan (2004), Continental geotherm and the evolution of continental margins, *Geology*, *32*, 133–136.

Russell, S. M., and R. B. Whitmarsh (2003), Magmatism at the west Iberia non-volcanic rifted continental margin: Evidence from analyses of magnetic anomalies, *Geophys. J. Int.*, *154*, 706–730.

Sayers, J., P. A. Symonds, N. G. Direen, G. Bernardel (2001), Nature of the continent-ocean transition on the non-volcanic rifted margin of the central Great Australia Bight, in *Non-Volcanic Rifting of Continental Margins: A Comparison of Evidence From Land and Sea*, edited by R. C. L. Wilson et al., *Geol. Soc. Spec. Publ.*, *187*, 51–76.

Schaltegger, U., L. Desmurs, G. Manatschal, O. Müntener, M. Meier, and D. Bernoulli (2002), The transition from rifting to seafloor spreading within a magma-poor rifted margin: Field and isotopic constraints, *Terra Nova*, *14*, 156–162.

Seyler, M., M. Cannat, and C. Mével (2003), Evidence for major-element heterogeneity in the mantle source of abyssal peridotites from the Southwest Indian Ridge (52° to 68°E), *Geochem. Geophys. Geosyst.*, *4*(2), 9101, doi:10.1029/2002GC000305.

Shillington, D. J., W. S. Holbrook, B. E. Tucholke, J. R. Hopper, K. E. Louden, H. C. Larsen, H. J.A. Van Avendonk, S. Deemer, and J. Hall (2004), Data report: Marine geophysical data on the Newfoundland nonvolcanic rifted margin around SCREECH Transect 2, in *Proc. Ocean Drill. Program*, Init. Rep. [CD-ROM], *210*, 1–39.

Sibuet, J.-C. (1987), Contribution à l'étude des mécanismes de formation des marges continentales passives, Doctorat d'Etat thesis, 351 pp., Univ. de Bretagne Occidentale, Brest, France.

Sibuet, J.-C., and X. Le Pichon (1971), Structure gravimétrique du golfe de Gascogne et le fossé marginal nord-espagnol, in *Histoire Structurale du Golfe de Gascogne*, edited by J. Debyser, X. Le Pichon, and L. Montadert, pp. 1–17, Technip, Paris.

Sibuet, J.-C., S. Monti, B. Loubrieu, J.-P. Mazé, and S. Srivastava (2004a), Carte bathymétrique de l'Atlantique nord-est et du golfe de Gascogne: Implications cinématiques, *Bull. Soc. Geol. Fr.*, *175*, 429–442.

Sibuet, J.-C., S. Srivastava, and W. Spakman (2004b), Pyrenean orogeny and plate kinematics, *J. Geophys. Res.*, *109*, B08104, doi:10.1029/2003JB002514.

Sibuet, J.-C., S. P. Srivastava, M. Enachescu, and G. Karner (2007), Early Cretaceous motion of Flemish Cap with respect to North America: Implications on the formation of Orphan Basin and S-E Femish Cap/Galicia Bank conjugate margins, in *Imaging, Mapping and Modelling Continental Lithosphere Extension and Breakup*, edited by G. Karner, G. Manatschal, and L. M. Pinheiro, *Geol. Soc. Spec. Publ.*, *282*, 59–92.

Skelton, A. D.L., and J. W. Valley (2000), The relative timing of serpentinization and mantle exhumation at the ocean-continent transition, Iberia: Constraints from oxygen isotopes, *Earth Planet. Sci. Lett.*, *178*, 327–338.

Spector, A., and F. S. Grant (1970), Statistical models for interpreting aeromagnetic data, *Geophysics*, *35*, 293–302.

Srivastava, S. P., and W. R. Roest (1995), Nature of thin crust across the southwest Greenland margin and its bearing on the location of the ocean-continent boundary, in *Rifted Ocean-Continent Boundaries*, *NATO ASI Ser., Ser. C*, edited by E. Banda, M. Torné, and M. Talwani, pp. 95–120, Kluwer Acad. Publ., Dordrecht, Netherlands.

Srivastava, S., J.-C. Sibuet, S. Cande, W. R. Roest, and I. R. Reid (2000), Magnetic evidence for slow seafloor spreading during the formation of the Newfoundland and Iberian margins, *Earth Planet. Sci. Lett.*, *182*, 61–76.

Tikku, A. A., and S. C. Cande (1999), The oldest magnetic anomalies in the Australian-Antarctic Basin: Are they isochrons?, *J. Geophys. Res.*, *104*, 177–661.

Toft, P. B., and S. E. Haggerty (1990), The effects of serpentinization on density and magnetic suceptibility: A petrophysical model, *Phys. Earth Planet. Inter.*, *65*, 135–157.

Tucholke, B. E., and J.-C. Sibuet (2007), Tectonic and sedimentary evolution of the Newfoundland-Iberia rift, in *Proc. Ocean Drill. Program Sci. Results*, *210*, in press.

Tucholke, B. E., D. S. Sawyer, and J.-C. Sibuet (2007), Breakup of the Newfoundland-Iberia rift, in *Imaging, Mapping and Modelling Continental Lithosphere Extension and Breakup*, *Geol. Soc. Spec. Publ.*, *282*, 9–42.

Urquhart, E. (2001), Depositional environment of syn-rift sediments on the Iberia margin, *EOS Trans. AGU*, *82*(47), Fall Meet. Suppl., Abstract 42B-0505.

Van der Voo, R. (1990), Phanerozoic paleomagnetic poles from Europe and North America and comparison with continental reconstructions, *Rev. Geophys.*, *18*, 167–206.

Verhoef, J., R. Macnab, and Project Team (1996a), Compilation of magnetic data in the Arctic and North Atlantic oceans, unpublished report, pp. 1–13, Bedford Inst. of Oceanogr., Dartmouth, Canada.

Verhoef, J., W. R. Roest, R. Macnab, J. Arkani-Ahmed, and Members of the Project Team (1996b), Magnetic anomalies of the Arctic and North Atlantic oceans and adjacent land areas, *Open File 3125*, Geol. Surv. of Can., Ottawa, Ontario, Canada.

Wessel, P., and W. M.F. Smith (1991), Free software helps map and display data, *Eos Trans. AGU*, *72*, 441, 445–446.

White, R. S., D. McKenzie, and K. O'Nions (1992), Oceanic crustal thickness from seismic measurements and rare earth element inversions, *J. Geophys. Res.*, *97*, 19,683–19,715.

Whitmarsh, R. B., P. Miles, J.-C. Sibuet, and V. Louvel (1996), Geological and geophysical implications of deep-tow magnetometer observations near ODP sites 897, 898, 899, 900 and 901 on the west Iberia continental margin, *Proc. Ocean Drill. Program Sci. Results*, *149*, 665–674.

Whitmarsh, R. B., M.-O. Beslier, P. Wallace, P. J. Fox, T. A. Davies, and T. J. G. Francis (1998), *Proceedings of the Ocean Drilling Program, Initial Reports*, vol. 173, Ocean Drill. Program, College Station, Tex.

Whitmarsh, R. B., G. Manatschal, and T. A. Minshull (2001a), Evolution of magma-poor continental margins from rifting to seafloor spreading, *Nature*, *413*, 150–154.

Whitmarsh, R. B., T. A. Minshull, S. M. Russell, S. M. Dean, K. E. Louden, and D. Chian (2001b), The role of syn-rift magnetism in the rift-to-drift evolution of the west Iberia continental margin: Geophysical observations, in *Non-Volcanic Rifting of Continental Margins: A Comparison of Evidence From Land and Sea*, edited by R. C. L. Wilson et al., *Geol. Soc. Spec. Publ.*, *187*, 107–124.

Wilson, R. C. L., G. Manatschal, and S. Wise (2001), Rifting along non-volcanic passive margins: Stratigraphic and seismic evidence from the Mesozoic successions of the Alps and western Iberia, in *Non-Volcanic Rifting of Continental Margins: A Comparison of Evidence From Land and Sea*, edited by R. C. L. Wilson et al., *Geol. Soc. Spec. Publ.*, *187*, 429–452.

Zhao, X. (1996), Magnetic signatures of peridotite rocks from sites 897 and 899 and their implications, in *Proc. Ocean Drill. Program Sci. Results*, *149*, 431–446.

Zhao, X. (2001), Palaeomagnetic and rock magnetic results from serpentinized peridotites beneath the Iberian Abyssal Plain, in *Non-Volcanic Rifting of Continental Margins: A Comparison of Evidence From Land and Sea*, edited by R. C. L. Wilson et al., *Geol. Soc. Spec. Publ.*, *187,* 209–234.

Zhao, X., B. Galbrun, H. Delius, and Q. Liu (2007a), Paleolatitude inferred from Cretaceous sedimentary and igneous cores recovered from leg 210, Newfoundland margin, in *Proc. Ocean Drill. Program Sci. Results*, *210*, in press.

Zhao, X., P. Riisager, M. Antretter, J. Carlut, P. Lippert, Q. Liu, B. Galbrun, S. Hall, H. Delius, and T. Kanamatsu (2007b), Unraveling the magnetic carriers of igneous cores from the Atlantic, Pacific, and the southern Indian oceans with rock magnetic characterization, *Phys. Earth Planet. Inter.*, in press.

G. Manatschal, CGS-EOST, Université Louis Pasteur, 1 rue Blessig, 67084 Strasbourg, France. (manatschal@illite.u-strasbg.fr)

J.-C. Sibuet, Département des Géosciences Marines, Ifremer Centre de Brest, B.P. 70, 29280 Plouzané, France. (jcsibuet@ifremer.fr)

S. Srivastava, Geological Survey of Canada, Bedford Institute of Oceanography, P.O. Box 1006, Dartmouth, N.S., Canada B2Y 4A2. (shirisrivastava@eastlink.ca)